FINAL REPORT

STUDY IMPROVEMENT OF THE HYDROGEN MASER

(30 July 1965 to 31 August 1966)

Contract No. NAS5-9888

Prepared by

varian
quantum electronics division
beverly/massachusetts

for

NATIONAL AERONAUTICS AND SPACE ADMINISTRATION

GODDARD SPACE FLIGHT CENTER, GREENBELT, MARYLAND

Final Report

STUDY IMPROVEMENT OF THE HYDROGEN MASER

January 18, 1967

Contract No. NAS5-9888

Period Covered:
30 July 1965 to 31 August 1966

Prepared by:

R.F.C. Vessot,
M.R. Baker and M.W. Levine

VARIAN ASSOCIATES
Quantum Electronics Division
Beverly, Mass.

for

GODDARD SPACE FLIGHT CENTER
National Aeronautics & Space Administration
Greenbelt, Maryland

TABLE OF CONTENTS

TABLE OF FIGURES

II. TECHNICAL DISCUSSION

A. THE THERMAL DISSOCIATOR

One of the important problems in the field of experimental atomic physics is the production of sufficiently intense beams of atoms or molecules when these are highly reactive or unstable, as are atomic hydrogen and free radicals. The use of electric discharges, such as in the Wood's discharge tube, has long been a favorite method, in particular when species with high excitation energies are required. More recently, with the availability of high-power radio frequency and microwave sources, discharges using r.f. excitation gained wide application.[1] The generation of the desired species in the electromagnetically-excited source is strongly dependent on the discharge conditions (power, frequency, gas pressure) and on surface effects on the discharge tube (recombination, quenching).

The hydrogen maser, as an atomic beam device, requires a source of atomic hydrogen which can deliver, after state selection in a magnet, 10^{12} to 10^{13} hydrogen atoms/sec. into the storage bulb in the maser cavity. In a practical laboratory instrument where operating time between maintenance periods is in part limited by pump capacity, it is desirable to obtain this working flux in the most efficient manner with respect to the total gas flux out of the source. For this purpose, sources are equipped with multi-tube collimators to furnish a highly directional flow from the source. (The collimator also allows the proper source pressure to be maintained for the currently-used r.f. discharge dissociator.) Proper design of the state-selecting magnet is important to maximize flux into the bulb, and the results of calculations to this end are presented in Section II-B.

The current r.f. discharge source has another characteristic which has given some difficulty in field applications. If a maser appears to require more atomic flux to oscillate properly, as in the case of a lower-than-usual cavity Q, a natural method is to increase hydrogen flow to the source and thus to raise the source discharge pressure. This has not infrequently resulted in the source developing a discharge condition known as "the whites," where the usual deep violet-red color of the discharge, characteristic of the Balmer series of atomic hydrogen, is

I. INTRODUCTION

The intent of the work done under this contract was to conduct a study involving both a scientific and an engineering approach to the improvement of the hydrogen maser for ease of operation and maintenance and for field use. Two particular technical areas were singled out as important. These were the atomic hydrogen dissociator and the tuning procedure required to put the maser into useful operating condition.

Work in these areas was begun in separate projects and in the course of studies related to these projects it became apparent that other problems of a more fundamental nature needed to be solved. These included magnet design and atomic trajectories in the state selecting system and also the design of the interaction region where the hydrogen atoms release their energy to the microwave field. Careful work in these areas had been somewhat neglected in earlier efforts to design and build the laboratory version of the hydrogen maser. From a general point of view as well as the more particular point of view included in the scope of this contract, these studies will aid considerably in the design of shorter, lighter, more efficient and more stable time and frequency standards for ground and space vehicle use.

replaced by a whitish-blue color, and in which little or no atomic hydrogen is produced. This pathological condition is not easy to cure and takes a considerable time (often days) to disappear. During this time, the maser does not operate, as hydrogen atom production in the white discharge is inadequate to maintain oscillation at all. Spectroscopic investigation of the light emitted by a source during the case of the whites shows the whitish color is due to the many-lined band spectra of molecular hydrogen. Details of this will be presented elsewhere, but the indication is that there is a change in the surface condition of the borosilicate glass walls of the source discharge tube under the higher pressure discharge, which leads to much more rapid recombination of atomic hydrogen into molecular hydrogen. This surface change is not easily reversed in a reliable manner.

The r.f. discharge source requires 10 to 20 watts of r.f. power at 200 MHz. If the maser is to be operated in the vicinity of highly sensitive communication equipment, extremely careful radiation shielding to prevent r.f. leakage is required.

The efficiency of the r.f. discharge source even in the absence of the pathological "whites" is highly dependent on the discharge condition, r.f. power, pressure, etc. While the literature indicates efficiencies as high as 90% dissociation, a more reasonable figure based on observations made in our laboratory is lower by as much as a factor of 5. In tuning the maser cavities, either manually or automatically (see Section II-C), the line Q is varied by changing the H flux into the bulb.[2] If one attempts to do this by changing the source pressure, atomic hydrogen flux changes, but in a way which is not strictly proportional to pressure. In an automatic tuning system where the proper feedback gain is determined by this change in hydrogen flux, if the source's efficiency varies at a given pressure because of, say, surface effects, the tuning correction increments will be non-optimal.

The preceding considerations suggested that an alternate approach to the production of atomic hydrogen for use in the maser, which would bypass the above-mentioned difficulties, could result in increased maser reliability and performance. Molecular hydrogen is dissociated into atomic hydrogen at elevated temperatures. The temperatures required are still far below those which would produce ionization, however. The degree of dissociation is determined only by the hydrogen pressure and temperature. Thus, in a thermal dissociation atomic hydrogen source,

the efficiency is known, as long as conditions of thermodynamic equilibrium prevail. The equilibrium constant for the dissociation is determined by the difference in free energy between the molecule and atom and may be obtained from standard thermodynamic tables.[3] Curves of dissociation efficiencies as a function of pressure and temperature are shown in Fig. A-1. Typically, a source at 2400°K and H_2 pressure of 20 microns is 90% efficient.

If a very large hydrogen atom flux is desired, the source pressure may be raised considerably, as long as the oven temperature is also raised to maintain dissociation efficiency. The practical limitation to this process is the vapor pressure of tungsten, which determines oven lifetime. The major disadvantage of a thermal dissociator is that the atoms emerge with the velocity characteristic of the oven temperature. Consequently, a longer state-selector magnet is required and the collection efficiency is reduced because of the smaller solid angle factor.

Thermal dissociation sources for atomic hydrogen have been made for atomic beam experiments previously; perhaps the best known use was in the classic experiments of W. Lamb and collaborators.[4] These were characterized by sizeable power consumption, water cooling and short lifetime. Both resistive heating and electron-bombardment heating have been used. The most recently reported source in the literature used resistive heating.[5] To test the feasibility of maser operation with a thermal dissociation source, a resistance-heated, water-cooled tungsten foil source was constructed. Many of the desirable features of a practical maser source were deliberately not included in this first test model. This is shown in Figure A-2.

It consists of a 1/8" diameter tube of six turns of 1 mil tungsten foil gripped on the ends with molybdenum holders. The ends of the tubing are forced outward by threaded conical molybdenum inserts. The end supports are cooled by conduction to copper blocks, which are water-cooled through ceramic-metal seals. Heating is accomplished by passing heavy alternating current through the tubing by means of the end supports. Hydrogen atoms emerge in a Lambert-law angular distribution through a simple hole in the middle of the tungsten foil tube. Because most of the atoms so emerging are at angles such as not to pass through the focussing magnet and into the maser storage bulb, differential pumping and separate beam collimation were used to decrease the load on the maser VacIon® pumps. The region is thus

® Registered, Varian Associates.

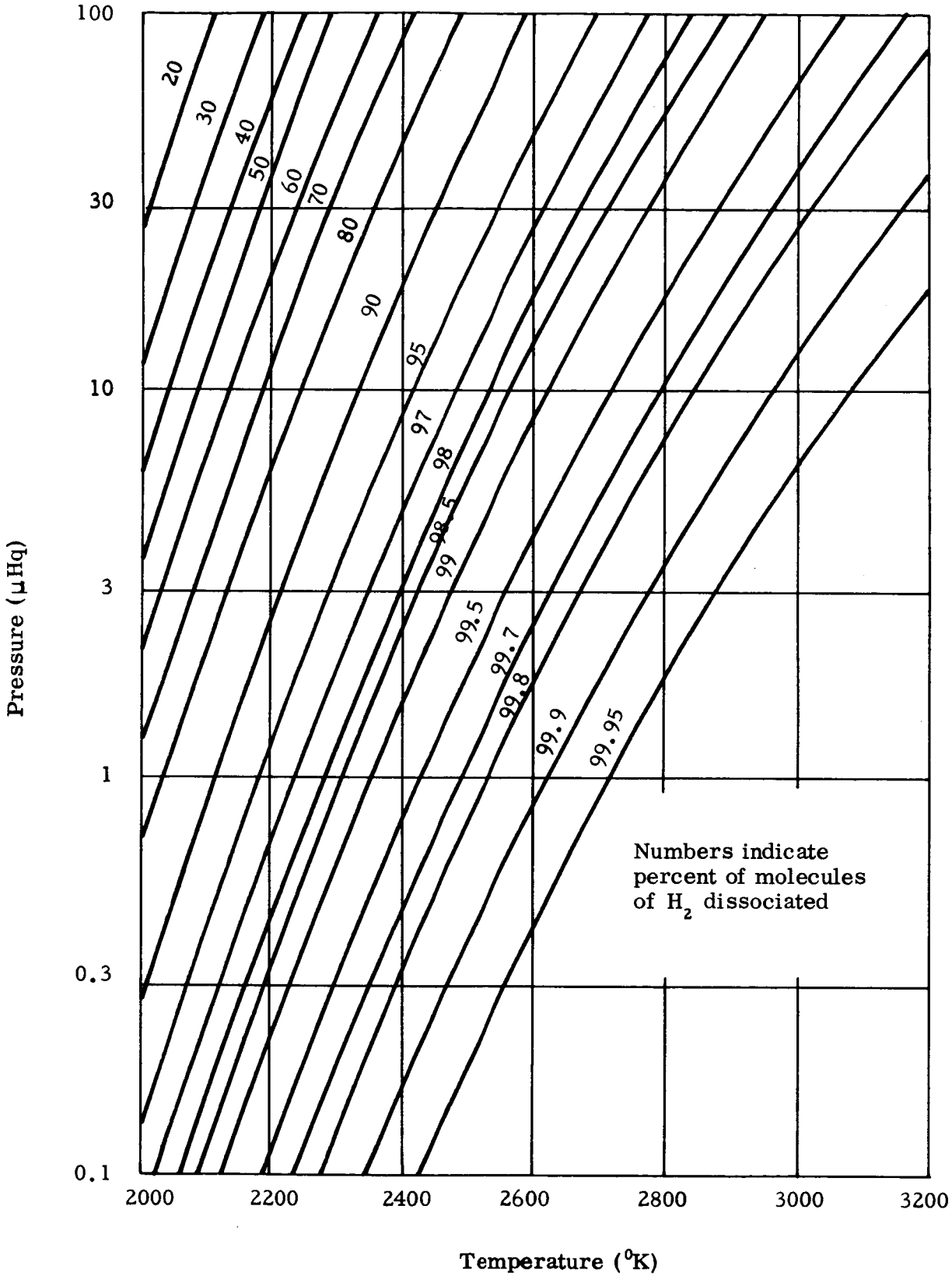

Fig. A-1. Calculated Dissociation Fraction.

Figure A-2. Thermal Dissociator Atomic Hydrogen Source.

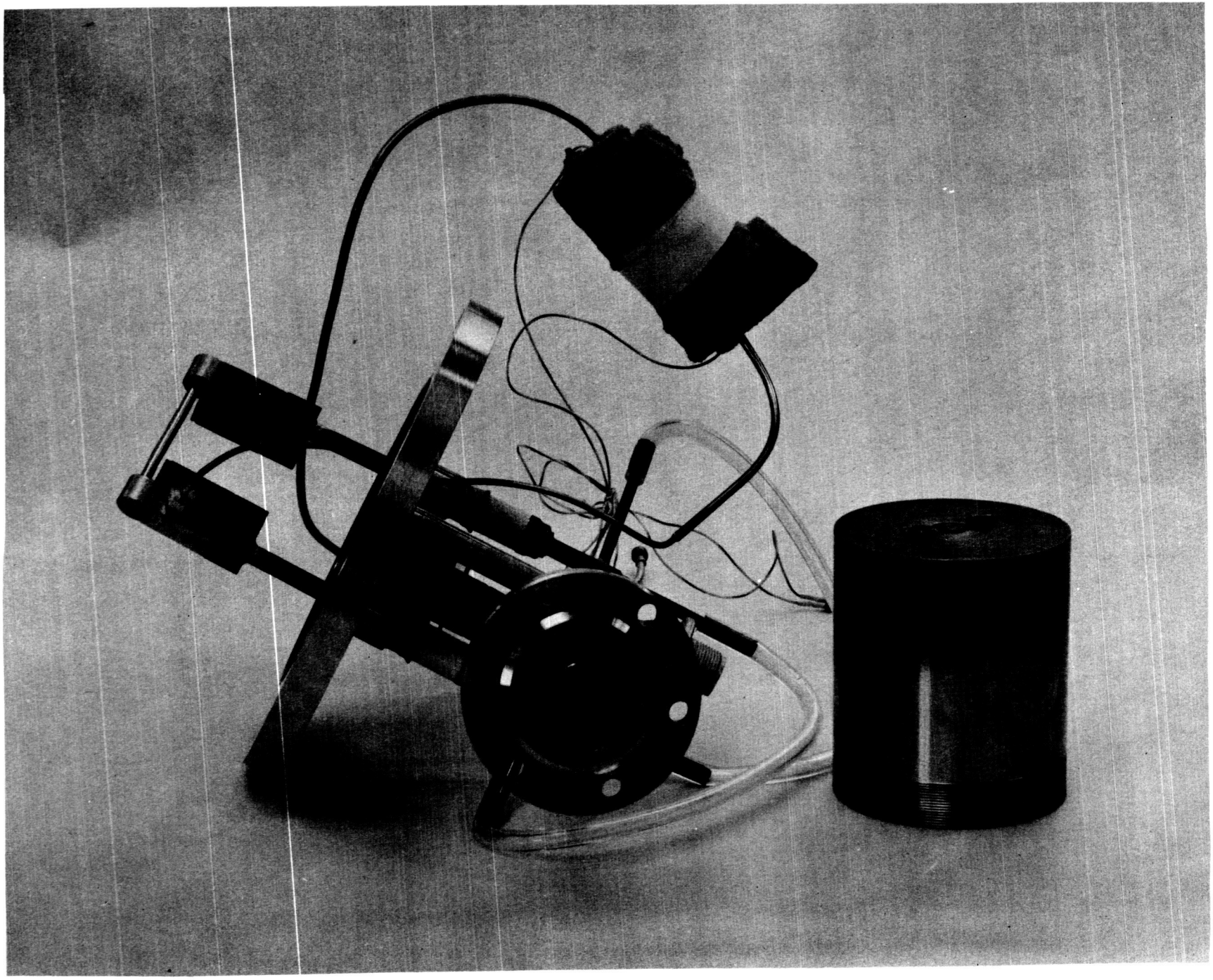

surrounded by a stainless steel capping tube which acts as a heat shield, pumping enclosure and collimator (shown in place in Fig. A-3). Hydrogen is introduced through a heated palladium leak and stainless steel tube into one end mount.

The device was placed in a hydrogen maser equipped with two focussing magnets in series to compensate for the higher velocity of the atoms emerging from the thermal source. The differential pumping enclosure was separately evacuated by a Welch 1397 mechanical pump. This experimental arrangement is shown in Fig. A-4. After alignment, the tungsten foil tube was heated by passing 60 cycle a. c. current through it while its temperature was monitored by means of an optical pyrometer. At a current of 150 amperes, the temperature of the center portion of the tube reached 2400^{0}C. At this temperature, a large percentage of the hydrogen molecules are dissociated into atoms, and maser oscillation was achieved. The temperature of the source was lowered to determine the oscillation threshold. With proper adjustment of hydrogen flow conditions, oscillation could be maintained at a temperature of 2000^{0}C. An intermediate temperature of 2400^{0}K was determined to be most satisfactory from the point of view of lifetime and hydrogen flow rate. The time required to turn up the source from room temperature was only three seconds, and the level of maser oscillation was easily varied by changing the source temperature. The maser was then permitted to oscillate for approximately 12 hours to determine if any deterioration would appear in the source. None was detected, and examination indicated that the source could probably have continued to function for a very long time.

Although the above described source was satisfactory as a laboratory experiment, it possesses four major disadvantages:

1) High power consumption -- 250 watts at 2400^{0}K;
2) Necessity for water cooling -- hence thermal inefficiency;
3) Need for an auxiliary mechanical pump;
4) High hydrogen consumption.

At the elevated temperatures required for dissociation, the major source of heat loss is through radiation. At 2500^{0}K, the power radiated by 1 cm.^{2}, emissivity = 1, is over 200 watts. It is hence advantageous in minimizing power consumption to have as small an area of the oven heated as possible. Heat loss by conduction to the supports must also be severely limited. The emergent atomic beam should be

Figure A-3. Thermal Dissociator Atomic Hydrogen Source, showing capping tube in place.

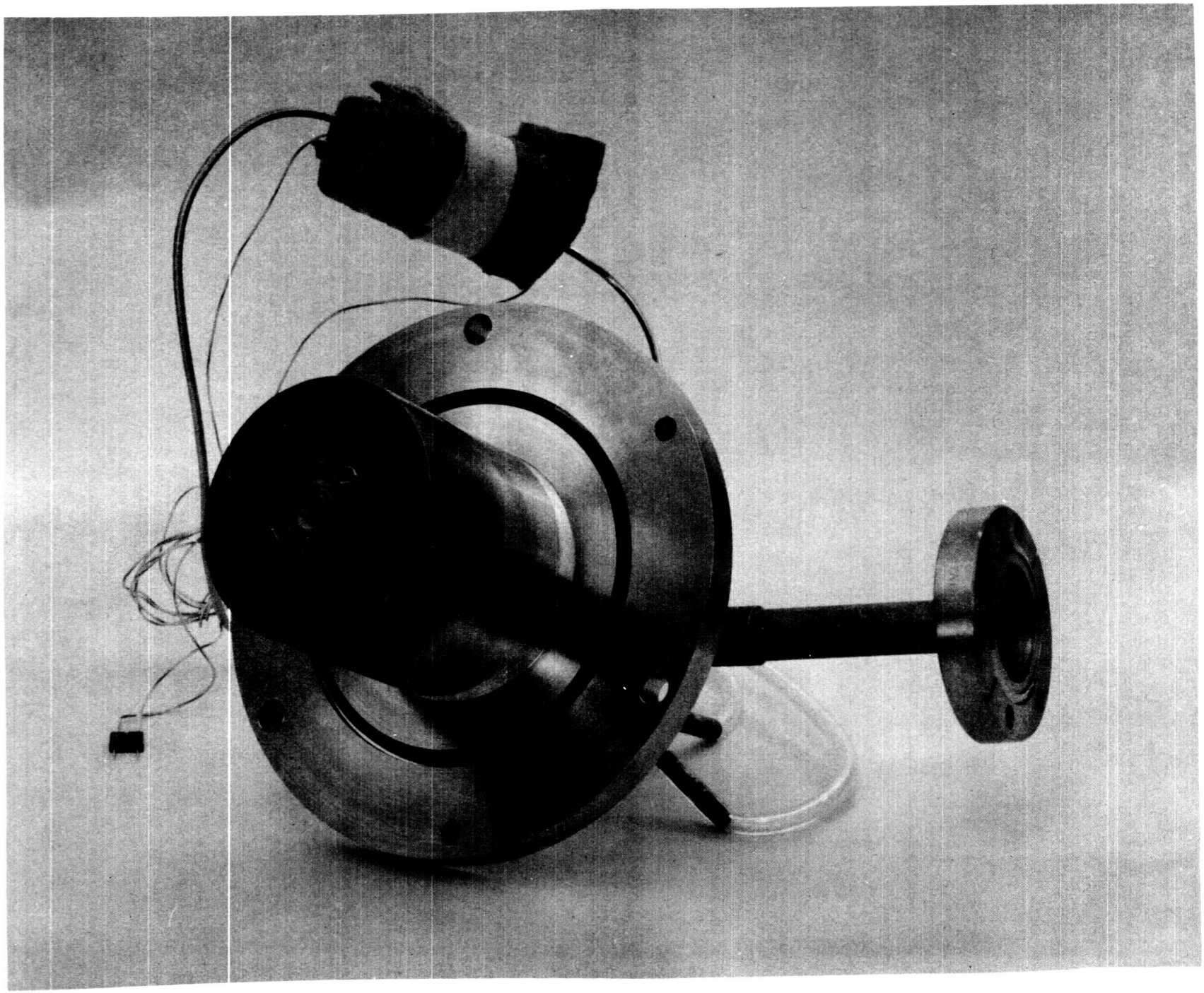

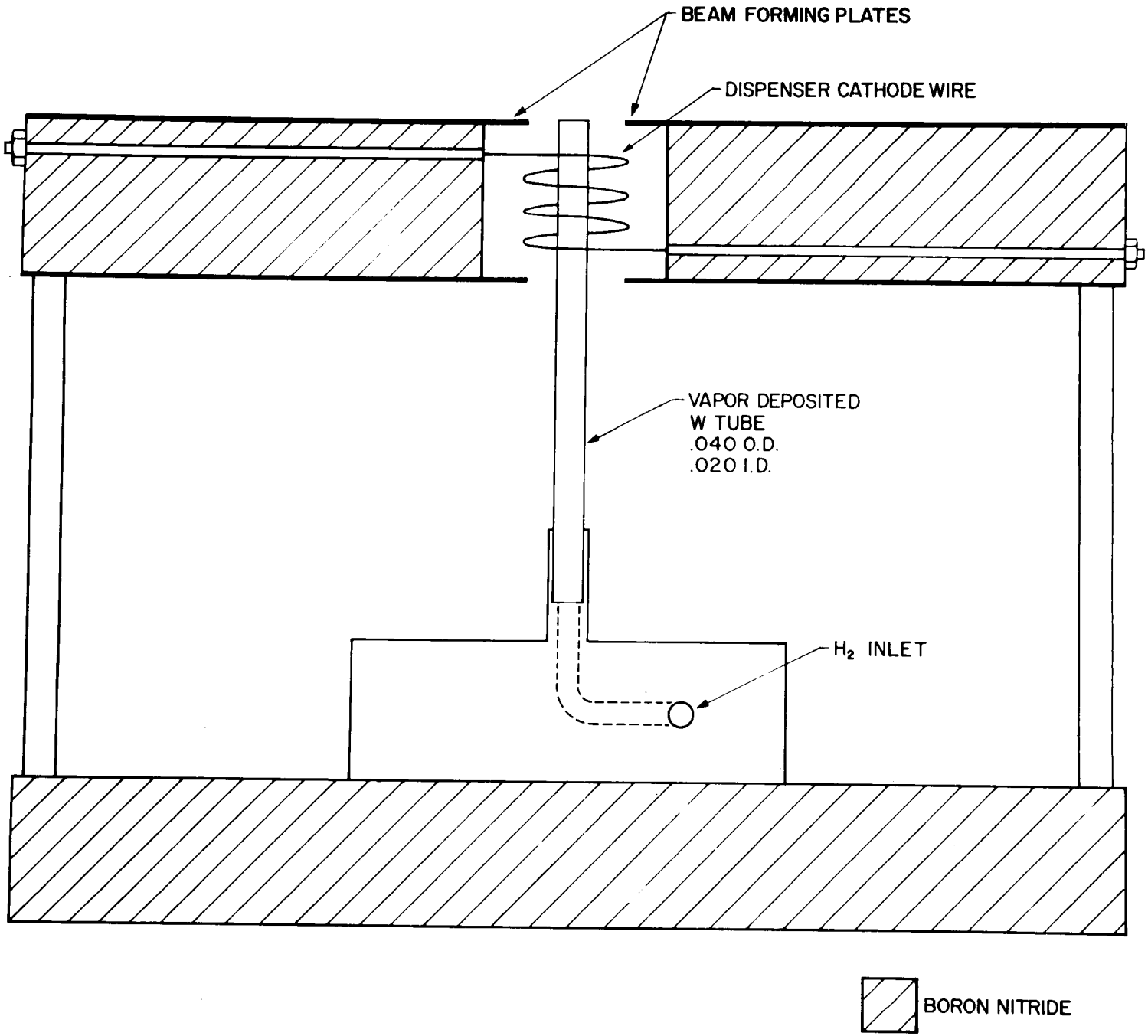

Figure A-5. ELECTRON BOMBARDMENT HEATED THERMAL DISSOCIATOR

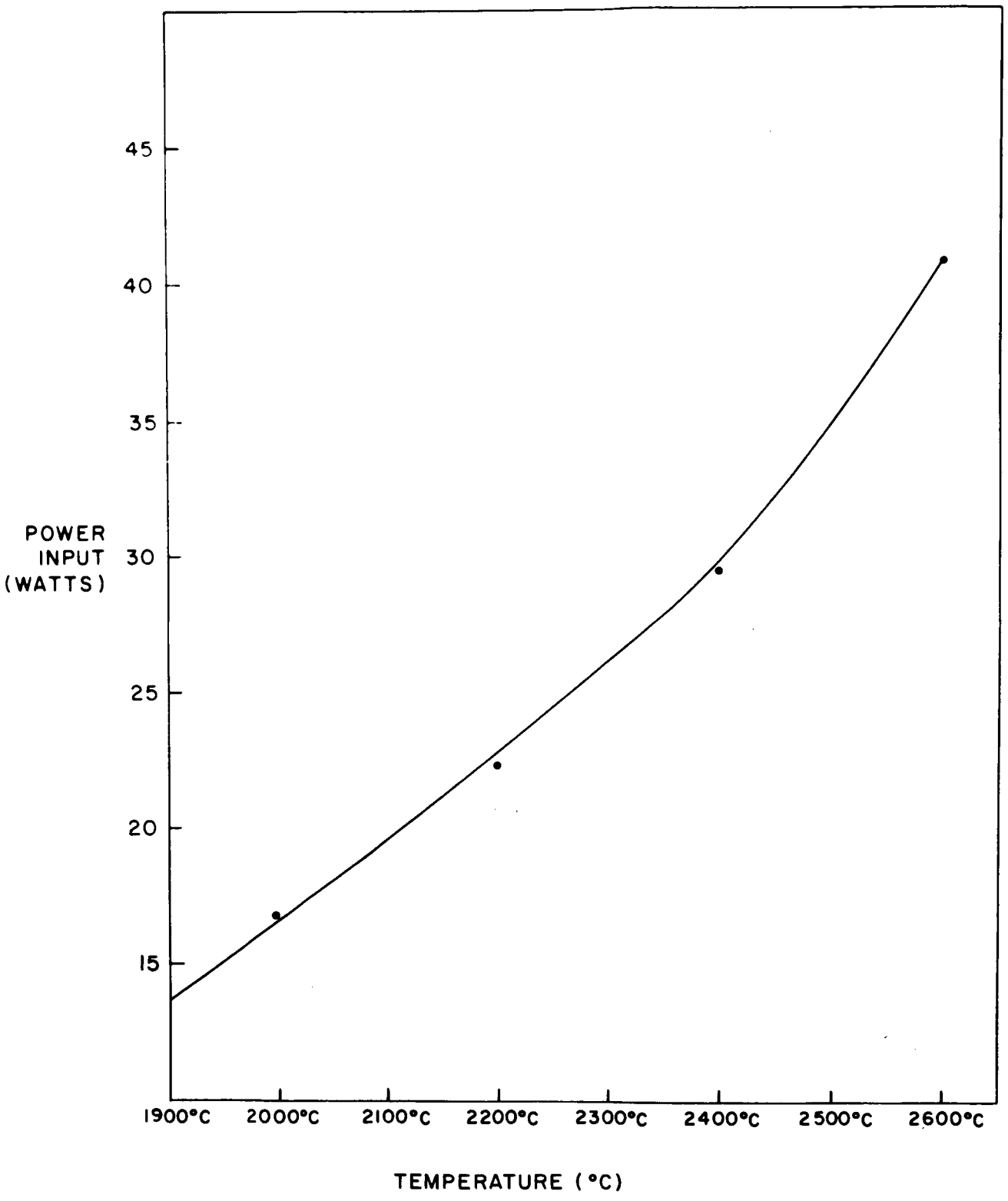

Fig. A-6. Power Input vs. Temperature for the Electron-Bombardment Heated Thermal Dissociator.

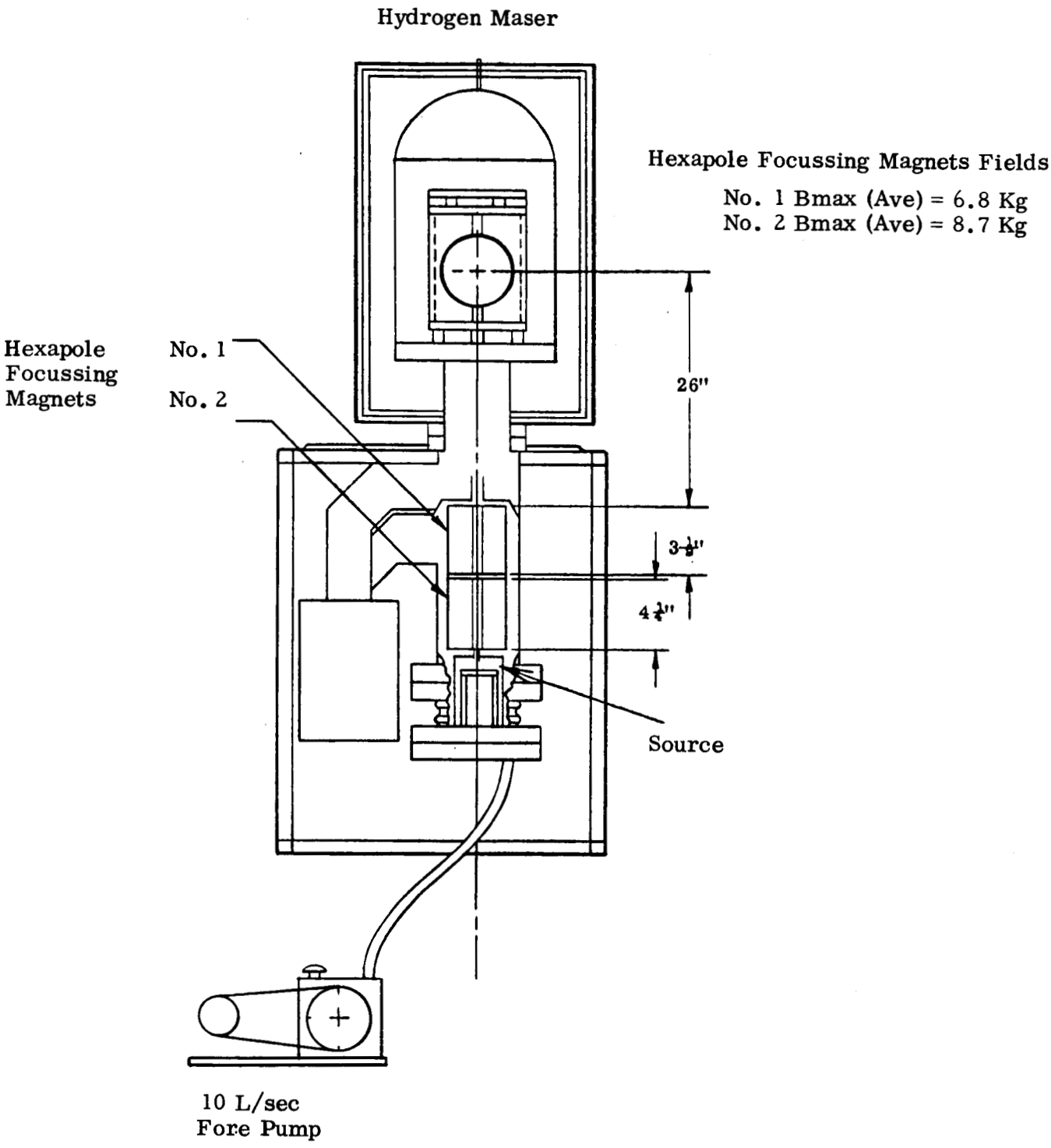

Fig. A-4. Experimental Apparatus.

highly directional to minimize vacuum pump load. Radiation loss should be contained and, if possible, reflected back through the use of radiation shields.

These considerations led after further experimentation to the design indicated schematically in Fig. A-5. It consists of a .040 O.D., .020" I.D. tungsten tube made by vapor deposition. The end of the tube from which the atoms emerge is heated by electron bombardment from a surrounding spiral wire dispenser cathode (experimental type, Varian). The surrounding electron beam assembly acts like a heat shield reducing radiation loss. The heated area of the tube is only about 1 cm. long, or about 20 inside diameters. The theoretical power lost by radiation for such a tube is 20 watts at 2500°K (total spectral emissivity of W = .303 at 2500°K). The conduction loss is minimized by using a long W tube, subject to the limitations of mechanical and vibration strength and supported on only one end. The long, thin tube produces an atomic beam whose angular distribution is highly peaked in the forward direction. The boron nitride block containing the electron gun assembly conducts heat easily down the support rods to the mounting flange. After proper activation of the cathode, electron emission may be maintained with less than 10 watts input. The temperature versus power input (electron beam current × accelerating voltage) is shown in Fig. A-6. This curve is fitted by the equation

$$P\ (\text{watts}) = .552 \left(\frac{T}{1000}\right)^4 + .625 \left(\frac{T}{1000} - .5\right) \quad \text{where } T \text{ is in } {}^0K.$$

At 2500°K, this shows that approximately 21 watts are radiated and 2 watts are lost by conduction down the tube, in excellent agreement with theoretical estimates. Under normal operating conditions in a maser, the total power input requirement is less than 30 watts and hence less than for the r.f. discharge source currently used in the Varian H-10 hydrogen maser. Dispenser cathodes may be reactivated after exposure to air several times and hence need not be replaced if vacuum is broken. The use of pure W for the oven material allows much higher temperature operation than the source described in reference 5, and our total source efficiency is three times higher (30 watts versus 90 watts at 2400°K).

Tests for ruggedness, reliability, lifetime and characteristics under a variety of operating conditions are continuing.

B. ATOMIC TRAJECTORIES

Hydrogen maser oscillation level is determined by the flux of hydrogen atoms in the $F = 1$, $m_F = 0$ state into the storage bulb. This state selection is accomplished by inhomogeneous magnetic fields which focus the desired hyperfine state into the bulb and defocus the undesired states. The flux depends on source pressure and temperature, magnet aperture and field strength, the source-bulb distance, and bulb aperture. In practice, the magnet field strength and aperture are limited by the materials from which it is constructed (saturation of pole-tips, energy density of Alnico). The temperature of the source affects the velocity distribution in the beam, with higher temperatures resulting in faster atoms which are more difficult to bend. This must be compensated for by using longer selection magnets.

Calculations have been carried out, using both machine and hand methods, of the trajectories of hydrogen atoms through magnetic fields of a hexapolar symmetry. Results have been obtained for the optimum length of focussing magnet, at the maximum practical field strength at the pole tips of about 10 kilogauss. A perfect hexapolar field has an intensity which varies as Kr^2, where r is the radial distance from the axis of the magnet. All the calculations to be described assume this field distribution.

The magnetic moment of the hydrogen atom in a particular magnetic sub-state m is described by the Breit-Rabi formula

$$W = -\frac{\Delta W}{4} - 2\,\mu_I\,H_o\,m \pm \frac{\Delta W}{2}\sqrt{1 + 2mx + x^2}$$

where

W	is the energy of the hydrogen atom
ΔW	is the hyperfine separation, 1420.405 MHz
μ_I	is the proton magnetic moment
H_o	is the external magnetic field

and

$$x = \frac{\left(-\mu_J/J + \mu_I/I\right)}{\Delta W} H_o$$

where x is 1 for H_o about 500 gauss.

$\frac{\partial W}{\partial H_o} = \mu_{eff}$ is the effective magnetic moment of the atom, and the force exerted on the hydrogen atom is $\mu_{eff} \cdot \frac{dH}{dr}$. The paths followed by the atoms can be obtained by stepwise numerical integration, and the total expected intensity at the entrance hole of the maser bulb obtained, relative to the source intensity.

The two focussed states of hydrogen are $F = 1$, $m = 1$ and $F = 1$, $m = 0$. For $m = 0$, the effective magnetic moment is a function of H_o, but approaches an asymptotic value for $x >> 1$. The effective moment for $m = 1$ is a constant even in zero field, and has the same value as the limiting value for the $m = 0$ state. Thus, if the trajectories of the atoms pass mostly through regions where $x >> 1$, such as off the hexapole axis, there is negligible difference between the trajectories for $m = 0$ and $m = 1$ states. We will consequently present a first trajectory calculation, assuming a constant magnetic moment ($m = 1$ case) and which can be solved analytically.

$W = \mu_o H_o \left(\frac{r}{r_o}\right)^2$ for a hexapole magnet where r_o is the radius of the bore of the magnet.

$$-\nabla W = F = ma = -2 \mu_o H_o \frac{r}{r_o^2}$$

$$\therefore \ddot{r} = a = -\frac{2 \mu_o H_o}{m r_o^2} r = -\omega^2 r$$

where

$$\omega^2 = \frac{2 \mu_o H_o}{m r_o^2} \quad \text{or} \quad \omega = \sqrt{\frac{2 \mu_o H_o}{m}} \frac{1}{r_o}$$

$$\therefore \ddot{r} + \omega^2 r = 0$$

$$r = C_1 \cos \omega t + C_2 \sin \omega t.$$

Placing the source at the entrance to the hexapole magnet on the central axis

$$\Rightarrow r = 0 \text{ at } t = 0 \Longrightarrow C_1 = 0$$

$$\therefore \dot{r} = C_2 \omega \cos \omega t$$

$\dot{r} = v \sin \beta$ at $t = 0$ where β is the angle the atom makes initially with the axis, v is its velocity.

$$\therefore C_2 = \frac{v \sin \beta}{\omega}$$

so that in the magnet

$$r = \frac{v \sin \beta}{\omega} \sin \omega t$$

Now, the distance x along the axis that the atom has travelled is given by

$$x = vt \cos \beta \text{ or } t = \frac{x}{v \cos \beta}$$

$$\therefore r = \frac{v \sin \beta}{\omega} \sin \frac{\omega x}{v \cos \beta}$$

$$\dot{r} = v \sin \beta \cos \frac{\omega x}{v \cos \beta}$$

At the end of the magnet, $x = \ell_2$, the radial velocity v_r is given by

$$v_r = v \sin \beta \cos \left(\frac{\omega \ell_2}{v \cos \beta} \right)$$

The atom now travels in a straight line making an angle ϕ with the axis after leaving the magnet until it reaches the entrance to the bulb, the drift distance being denoted by ℓ_3. With $\frac{v_r}{v_x} = \tan \phi$, one obtains the final value of the radius at which the atom arrives at the end of the drift region,

$$r_f = \frac{v \sin \beta}{\omega} \sin \left(\frac{\omega \ell_2}{v \cos \beta} \right) + \ell_3 \tan \beta \cos \left(\frac{\omega \ell_2}{v \cos \beta} \right) \qquad \text{Equation (1)}$$

For small angles, $\beta << 1$, this expression becomes

$$r_f = \frac{v \beta}{\omega} \sin \left(\frac{\omega \ell_2}{v} \right) + \ell_3 \beta \cos \left(\frac{\omega \ell_2}{v} \right) \qquad \text{Equation (2)}$$

The condition for an atom to be refocussed onto the axis is $r_f = 0$, which occurs for a velocity v_o such that:

$$- \tan \left(\frac{\omega \ell_2}{v_o} \right) = \frac{\omega \ell_3}{v_o} \qquad \text{Condition 1}$$

An important fact to note is that

$$\beta = \frac{r_f}{\frac{v}{\omega} \sin \frac{\omega \ell_2}{v} + \ell_3 \cos \frac{\omega \ell_2}{v}} \qquad \text{Equation (3)}$$

For atoms which just graze the magnet, either within the magnet or at its end, the maximum allowable angle is

$$\beta_{max} = \frac{\omega r_o}{v} \qquad \text{Equation (4)}$$

To illustrate the use of these results let us consider the case of focussing into an aperture whose radius is equal to the magnet bore. This is shown in Fig. B-1. The velocity of the atoms focussed on the center of the aperture is given by v_o. The trajectory followed by an atom with a velocity higher than v_o (which is given by Condition 1) follows path 2, which in this limiting case grazes the end of the magnet and moves parallel to the axis on emerging. This velocity, which we denote by v_{max}, is given by

$$\frac{\omega \ell_2}{v_{max}} = \frac{\pi}{2} \qquad \text{Condition 2}$$

On the other hand, a slower atom, indicated by path 1 can make a larger initial angle with the axis, is bent over, and manages still to enter the aperture at $r_f = -r_o$. Its velocity, v_{min}, is given by the condition

$$-r_f = \left(\frac{v_{min}}{\omega}\right)\left(\frac{\omega r_o}{v_{min}}\right) \sin\left(\frac{\omega \ell_2}{v}\right) + \ell_3\left(\frac{\omega r_o}{v_{min}}\right)$$

or

$$-\frac{r_f}{r_o} = \sin\left(\frac{\omega \ell_2}{v}\right) + \frac{\omega \ell_3}{v_{min}} \cos\left(\frac{\omega \ell_2}{v_{min}}\right) \qquad \text{Condition 3}$$

It may readily be determined that v_o as given by Condition 1 always lies between the values of v_{max} and v_{min} as given by Conditions 2 and 3.

It is also possible for a faster moving atom to get to the aperture through the magnet without grazing the pole-pieces. Such a possible path is shown by path 3 in Fig. B-1. The maximum initial angle β which such atoms can make with the axis is determined by Equation 3.

The intensity distribution of atoms as a function of velocity for an atomic beam source is given by

$$I(v)\,dv = \frac{2I_o}{\alpha^4} v^3 e^{-v^2/\alpha^2}\,dv$$

where $\alpha = \sqrt{\frac{2kT}{m}}$. In such a beam source, the most probable velocity equals

$$\sqrt{\frac{3}{2}}\,\alpha = \frac{3kT}{m} = 1.22\,\alpha$$

[For atomic hydrogen at about 70°C, $\alpha = 2.5 \times 10^5$ cm/sec and $1.22\,\alpha = 3.05 \times 10^5$ cm/sec.]

The included solid angle intensity factor is given by ρ^2_{max}. This can easily be seen as follows:

The solid angle differential is $d\Omega = \sin\theta\, d\theta\, d\varphi$. Normalized to a hemisphere

$$\frac{d\Omega}{\Omega_{tot}} = \frac{\sin\theta\, d\theta\, d\varphi}{2\pi}$$

For a beam source following the Lambert law,

$$dI = 2I_0 \cos\theta \frac{d\Omega}{\Omega tot}$$

$$\int dI = I_0 \int_0^{2\pi} \int_0^{\pi/2} 2\cos\theta \sin\theta\, d\theta\, d\varphi \frac{1}{2\pi}$$

$$= I_0$$

$$\int dI \text{ for } \theta = 0 \text{ to } \rho_{max}$$

$$I = \int dI = I_0 \cos^2\theta \Big]_{\rho_{max}}^{0}$$

or $$\frac{I}{I_0} = 1 - \cos^2\rho_{max} = \rho^2_{max} \text{ for small } \rho_{max}$$

Hence, the expected intensity for a given velocity relative to the total source flux is

$$\frac{I(v)}{I_0} = \frac{2}{\alpha^4} v^3 e^{-v^2/\alpha^2} \rho^2_{max}$$

where ρ_{max} is itself a function of velocity.

In the case where the maser bulb aperture is larger than the magnet gap, the values of v as given by Conditions 1, 2, and 3 still hold, but a further type of trajectory becomes possible. This is shown as path 1 in Fig. B-2. This is where the atom just grazes the end of the magnet, continues in an upward direction, and enters the aperture. In this case, denoting the maximum allowed velocity by $v^{(2)}_{max}$,

$$r_o = \beta \frac{v}{\omega} \sin \frac{\omega \ell_2}{v} \quad \text{or} \quad \beta_{max} = \frac{\omega r_o}{v} \frac{1}{\sin\left(\frac{\omega \ell_2}{v}\right)}$$

Since

$$r_f = \beta\left[\frac{v^{(2)}_{max}}{\omega} \sin \frac{\omega \ell_2}{v^{(2)}_{max}} + \ell_3 \left(\frac{\omega \ell_2}{v^{(2)}_{max}}\right)\right]$$

$$r_f = r_o + \frac{\omega r_o}{v^{(2)}_{max}} \ell_3 \cot\left(\frac{\omega \ell_2}{v^{(2)}_{max}}\right)$$

or

$$\frac{r_f - r_o}{r_o} = \frac{\omega \ell_3}{v^{(2)}_{max}} \cot\left(\frac{\omega \ell_2}{v^{(2)}_{max}}\right) \qquad \text{Condition 4}$$

This reduces to Condition 2 if $r_f = r_o$. Denoting the different regimes of velocities as v_o (Condition 1); $v^{(1)}_{max}$ (Condition 2); v_{min} (Condition 3) and $v^{(2)}_{max}$ (Condition 4) and using the relevant expressions for the total integrated intensity into the aperture:

$$\frac{I}{I_o} = \frac{2}{\alpha^4} \int_{v_{min}}^{v^{(1)}_{max}} v^3 e^{-v^2/\alpha^2} \frac{\omega^2 r_o^2}{v^2} dv + \frac{2}{\alpha^4} \int_{v^{(1)}_{max}}^{v^{(2)}_{max}} v^3 e^{-v^2/\alpha^2} \frac{\omega^2 r_o^2}{v^2} \frac{dv}{\sin^2\left(\frac{\omega \ell_2}{v}\right)}$$

$$+ \frac{2}{\alpha^4} \int_{v^{(2)}_{max}}^{\infty} dv\, v^3 e^{-v^2/\alpha^2} \frac{r_f^2 \frac{\omega^2}{v^2}}{\left[\sin\left(\frac{\omega \ell_2}{v}\right) + \frac{\omega \ell_3}{v} \cos\left(\frac{\omega \ell_2}{v}\right)\right]^2}$$

$$+ \frac{2}{\alpha^4} \int_{\text{cut-off}}^{v_{min}} v^3 e^{-v^2/\alpha^2} \frac{r_f^2 \frac{\omega^2}{v^2} dv}{\left[\sin\left(\frac{\omega \ell_2}{v}\right) + \frac{\omega \ell_3}{v} \cos\left(\frac{\omega \ell_2}{v}\right)\right]^2} \qquad \text{Equation (5)}$$

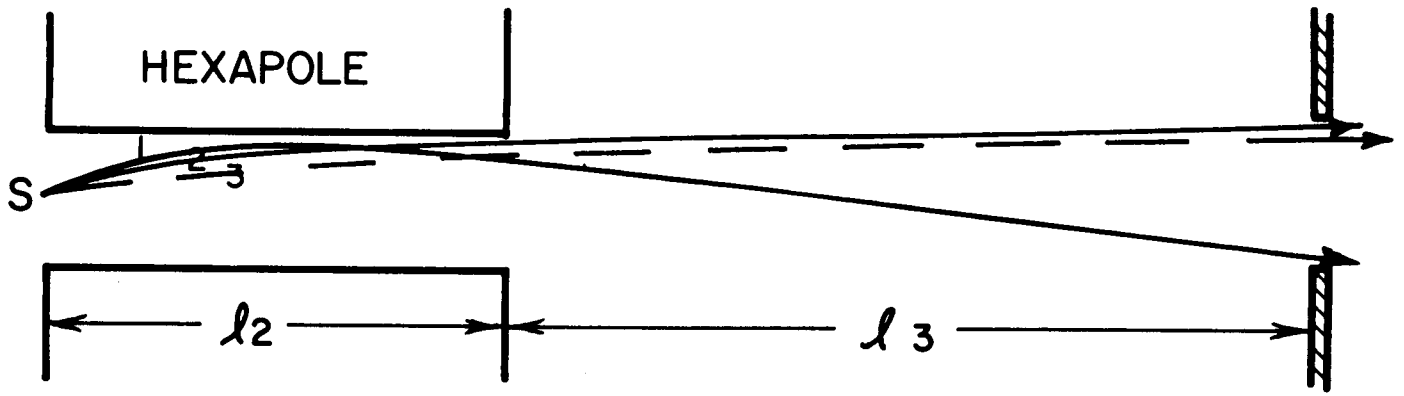

Fig. B-1. Focussing diagram, aperture radius = magnet gap.

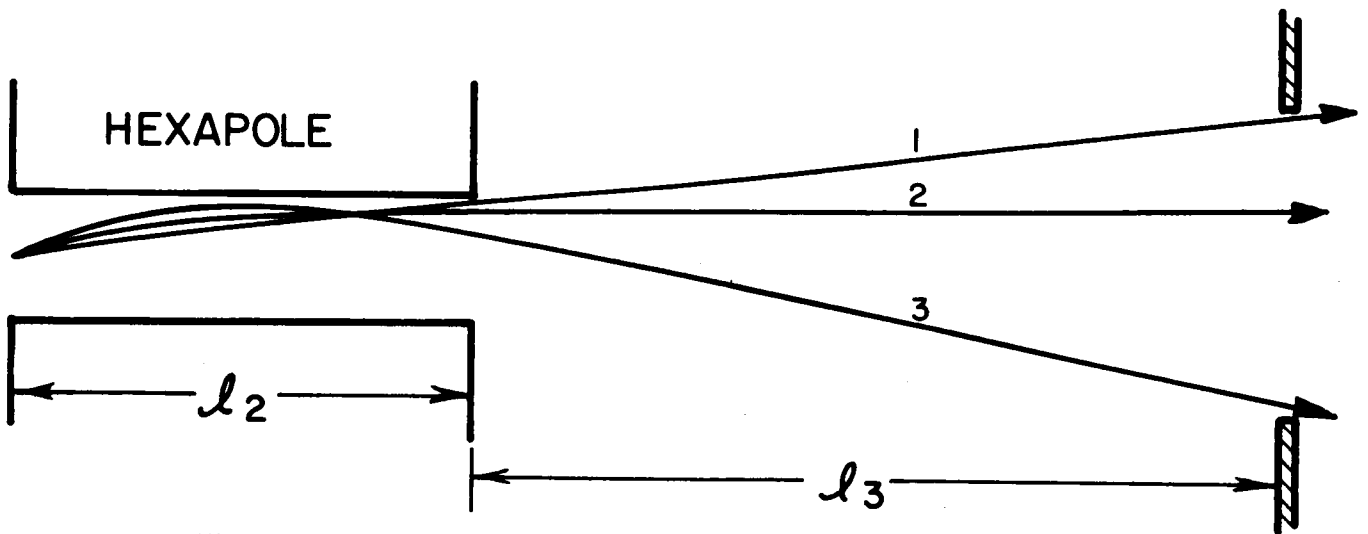

Fig. B-2. Focussing diagram, aperture radius > magnet gap.

where the low-velocity cut-off is introduced to exclude multiple-bend trajectories in the magnet which make negligible contribution to the total intensity.

The first integrand reduces to the simple functional form

$$\frac{\omega^2 r_o^2}{\alpha^2}\left[\left(\frac{v}{\alpha}\right) e^{-(v/\alpha)^2} \quad d\,(v/\alpha)\right]$$

which is the product of a constant solid angle factor and a normalized modified maxwellian distribution.

These results may be applied to the design and performance prediction of a practical selector magnet for a hydrogen maser. We choose the following design parameters. We have a hexapole magnet whose bore diameter is .125", maximum field at pole tips 9.5 K gauss, a distance ℓ_3 between magnet and bulb of 10", and a bulb aperture diameter of .2" ($r_f = 1.6\, r_o$). We determine what length magnet to use, what the intensity into the bulb is as a function of velocity, and the total expected flux.

Source temperature is 70°C. (R F. discharge atomic hydrogen source).

$$\alpha = 2.5 \times 10^5 \text{ cm/sec}$$

Setting $v_o = 1.22$ (focussed velocity = most probable beam velocity), and using Condition 1, we obtain

$$3.37 \times 10^{-2} \times 160 = -\tan\left(3.37 \times 10^{-2} L_2\right)$$

or

$$L_2 = 52.05$$

$$\ell_2 = 3.25 \text{ inches.}$$

Here, L_2 and L_3 are $\frac{\ell_2}{r_o}$ and $\frac{\ell_3}{r_o}$.

Condition 3 gives

$$-1.6 = \sin\frac{\omega \ell_2}{v_{min}} + \frac{\omega \ell_3}{v_{min}} \cos\frac{\omega \ell_2}{v_{min}}$$

An iterative solution of this transcendental equation gives:

$$v_{min} = 2.6856 \times 10^5 \text{ cm/sec} = 1.0742\, \alpha$$

Condition 2 gives $v^{(1)}_{max} = 1.3633\ \alpha$

Condition 4 gives $v^{(2)}_{max} = 1.4918\ \alpha = 3.7295 \times 10^5$ cm/sec.

One may plot the results using Equation 5 to obtain the curve shown in Figure B-3. The central portion of the curve in Fig. B-3 follows the ve^{-v^2/α^2} distribution. The curve may be integrated in part analytically (between v_{min} and $v^{(1)}_{max}$) and in part numerically to obtain the ratio of beam into the bulb to total beam $I/I_o = \frac{1.76}{\pi} \times 10^{-3}$. The relative contributions of the different parts of the velocity distribution are

$v < v_{min}$ - 19.2%

$v_{min} < v < v^{(2)}_{max}$ - 62.67%

and

$v^{(2)}_{max} < v$ - 18.13%

Computer-integrated trajectories were obtained for several magnet lengths and for source temperatures of 370°K and 2800°K (r.f. and thermal dissociators). The computer integrated the atom trajectory through the magnet, using the exact Breit-Rabi formula to determine the force on the atom along the path, for a particular velocity, and with the source located at the entrance of the magnet on axis. By stepping up the angle and integrating a new trajectory, the program determines the maximum allowable angle β_{max} for an atom to pass through the focussing magnet and to enter the bulb aperture, whose diameter equals the magnet aperture and is located at a given distance from the end of the magnet. The size of a beam stop located at the end of the focussing magnet is adjusted to prevent undeflected particles from the source (such as hydrogen molecules) from entering the bulb. This stop determines the minimum allowable angle β_{min} for a "good" trajectory. The solid angle factor as derived above is here given by $(\beta^2_{max} - \beta^2_{min})$. In practice, the β^2_{min} term is negligible. This calculation was repeated for a number of different velocities. The intensity as determined by the velocity distribution and solid angle was computed. The total intensity was then determined by evaluating the sum:

T = 370°K, magnet length = 4" (Fig. B-6)
T = 2800°K, magnet length = 6.25" (Fig. B-7)
T = 2800°K, magnet length = 9.375" (Fig. B-8)

The computer output data which is graphically shown in Figures B-4 through -8 is reproduced in Figs. B-9 through -13 in sequence.

We have thus determined the total relative bulb flux as a function of magnet length. The values of 3 inches and 8 inches for the r.f. discharge and thermal dissociator sources respectively are close to the optimal values for a 9.5 K gauss field at the pole tip. A change in magnet length from 3 inches to 4 inches for the r.f. discharge source decreases the flux at the bulb aperture by as much as 50%, so that these calculations have yielded important design information for the state selector. The excellent agreement between the exact computer calculation and hand calculations in the constant magnetic moment approximation gives us confidence in applying these methods to other experimental configurations.

For the beam source following Lambert's law as above, the intensity in the forward direction ($\theta = 0$) is $2I_o$. If a multitube collimator of the same exit area is used, the beam intensity in the forward direction is unaffected, while the intensity at larger angles is reduced. The reduction factor for the total flux is commonly denoted by K (the kappa factor). Thus, the ratio $\frac{I}{I_o}$ which is calculated may be easily modified to give the ratio of bulb flux to total source flux when a collimated source is used by simply multiplying the numerical values of I/I_o by the source K factor.

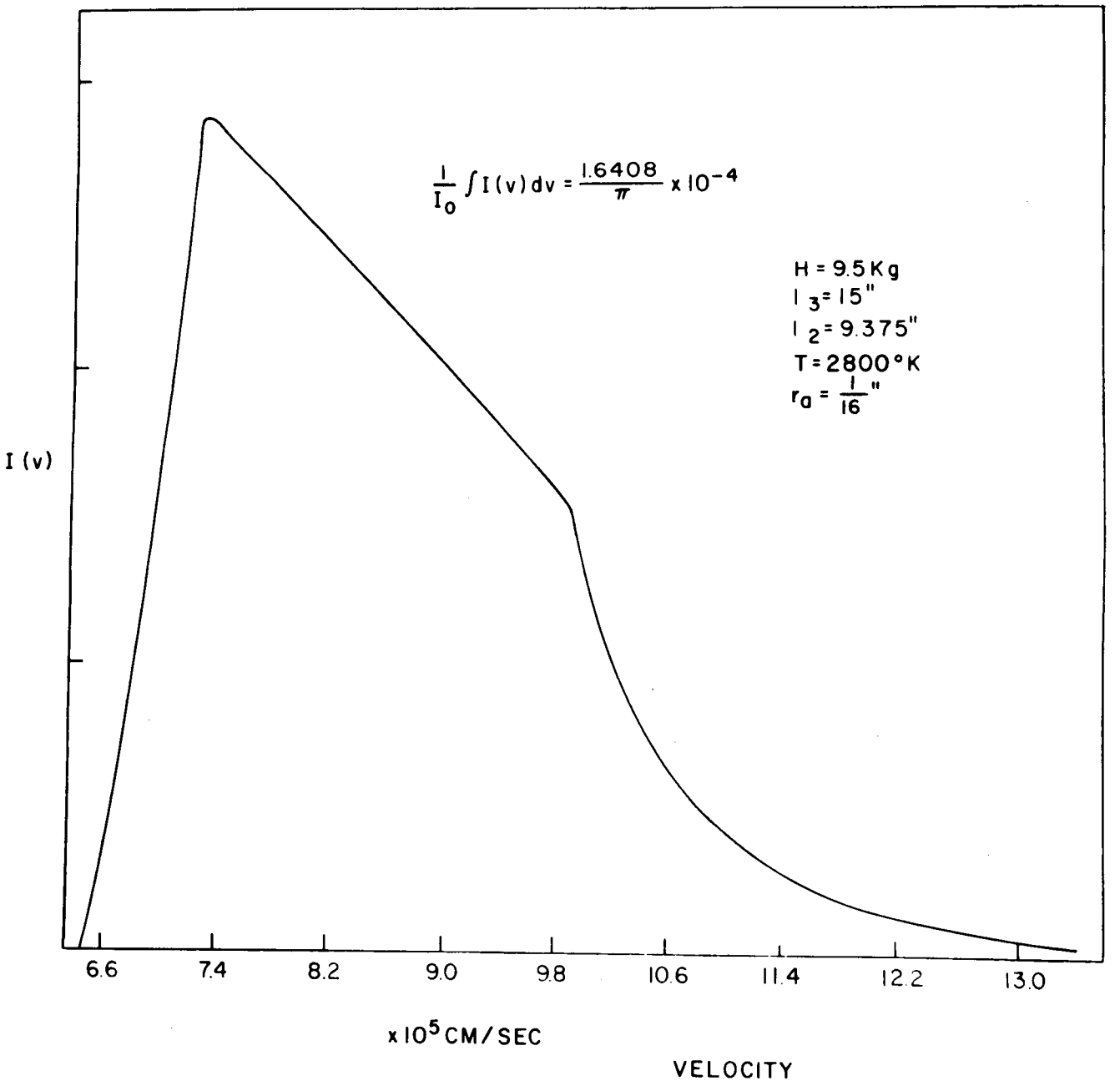

Fig. B-8. Intensity vs. Velocity curve, 9.375" Magnet, Thermal Dissociator.

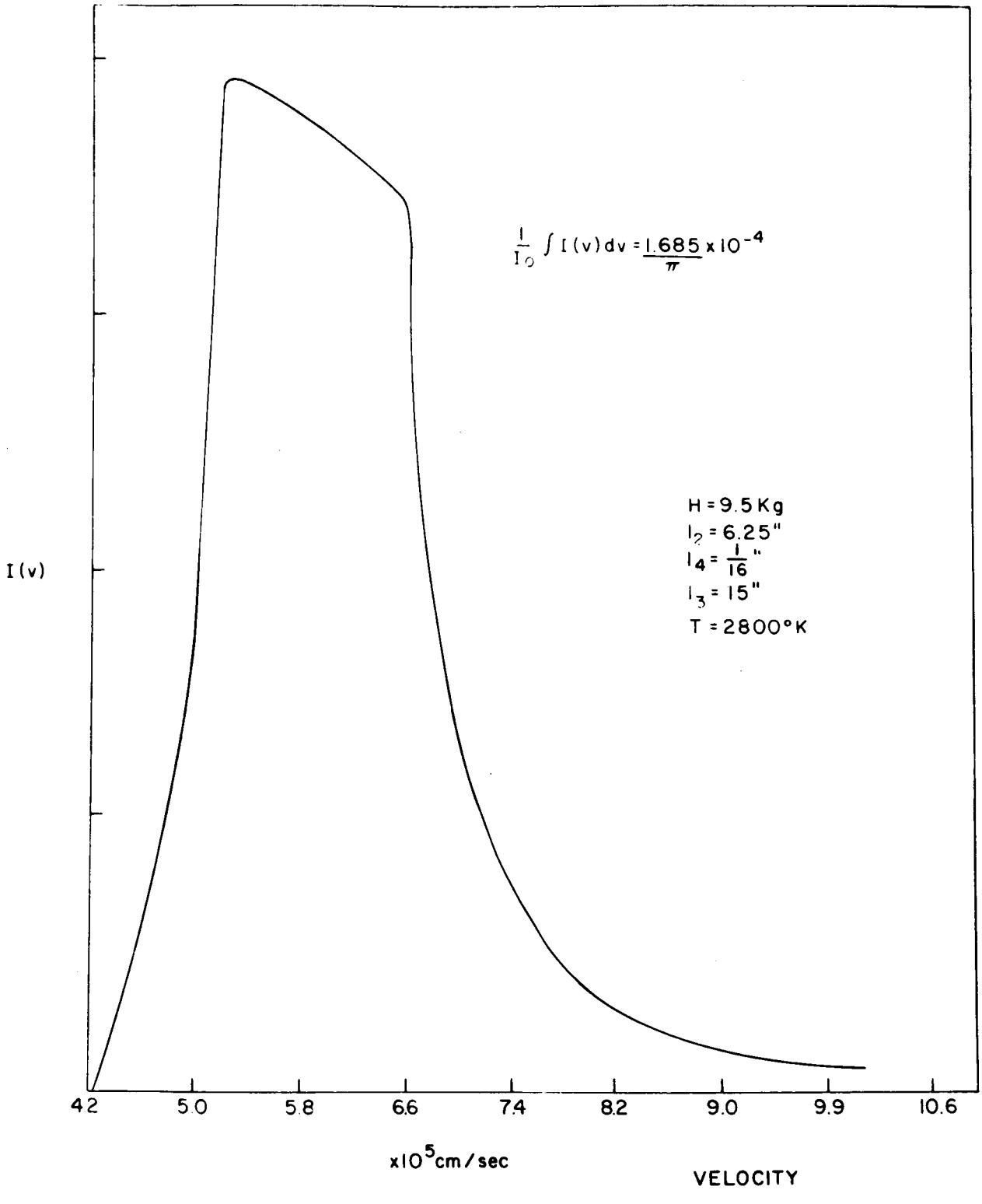

Fig. B-7. Intensity vs. Velocity curve, 6.25" Magnet, Thermal Dissociator.

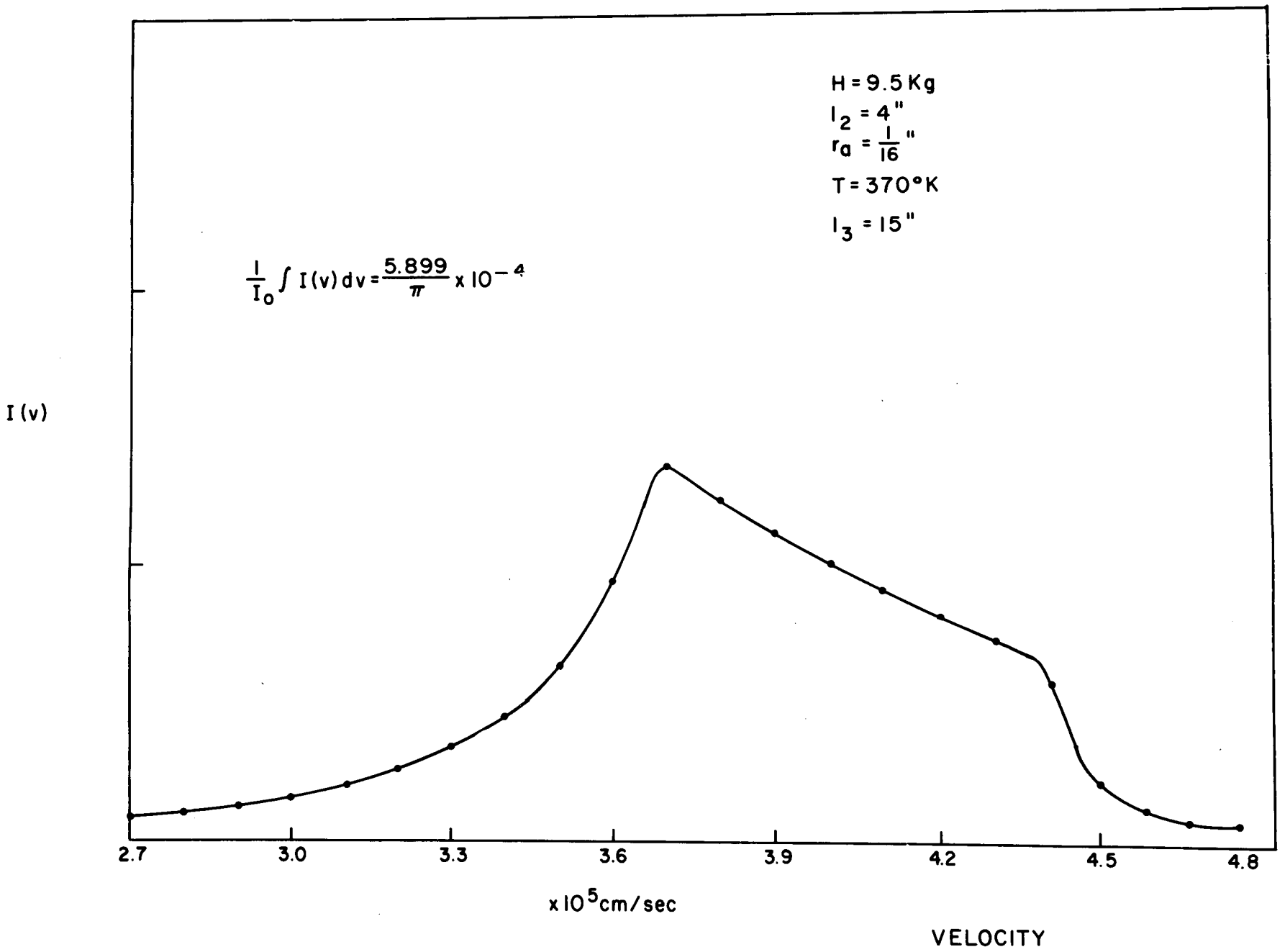

Fig. B-6. Intensity vs. Velocity curve, 4" magnet, r.f. dissociator.

$$\frac{S}{\pi} = \frac{I}{I_0} = \sum_i \frac{2}{\alpha^4} v_i^3 e^{-v^2/\alpha^2} \Delta v_i \left(\beta^2_{max} - \beta^2_{min} \right)$$

The computer output lists v_i, β_{max} and β_{min} (in degrees), $\pi (\beta^2_{max} - \beta^2_{min})$, the i'th term in the above sum, and S.

Fig. B-4 shows the results for an r.f. discharge atomic hydrogen source, magnet length 3". The bulb aperture is at a distance of 15" from the magnet and its diameter is equal to the magnet bore. It can be seen that the curves for m = 1 and for m = 0 are very similar. The total relative intensity for the m = 1 state is $\frac{8.324}{\pi} \times 10^{-4}$, while for m = 0, it is $\frac{7.853}{\pi} \times 10^{-4}$. One should expect slightly better focussing for m = 1 because of its constant effective magnetic moment. The population distributions are:

m = 0	$32\% < v_{min}$
	$9\% > v_{max}$
	59% for $v_{min} < v < v_{max}$
m = 1	$17\% < v_{min}$
	$25\% > v_{max}$
	58% for $v_{min} < v < v_{max}$

Thus, as in the analytic result, approximately 60% of the atoms have velocities between v_{min} and v_{max} and 40% lie in the "tails."

Fig. B-5 shows an intensity versus velocity distribution curve for a thermal dissociator atomic hydrogen source, where the atoms emerge with a velocity corresponding to 2800°K. The magnet length has been increased to 8 inches to focus the higher velocity distribution from the high temperature source. Because of the reduction in available solid angle in the longer magnet, the total relative intensity into the bulb is $\frac{1.825}{\pi} \times 10^{-4}$, considerably smaller than with the r.f. discharge source. This could be compensated for experimentally by increasing the total flux, a process which can be done easily for the thermal source.

Figs. B-6, -7, and -8 show the m = 0 bulb flux as a function of velocity with the bulb 15 inches from the end of the magnet, and under the following conditions:

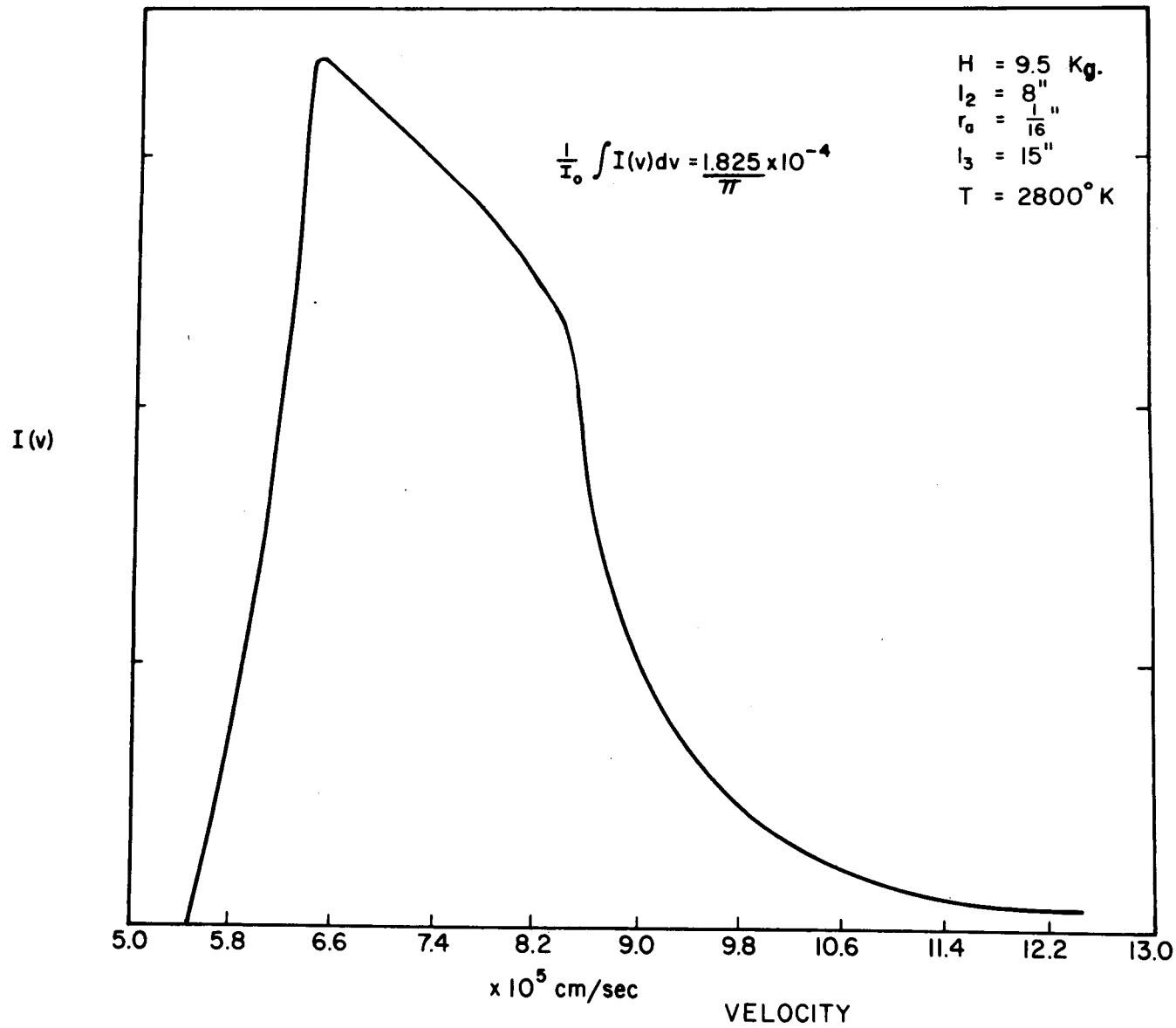

Fig. B-5. Intensity vs. Velocity curve, thermal dissociator source.

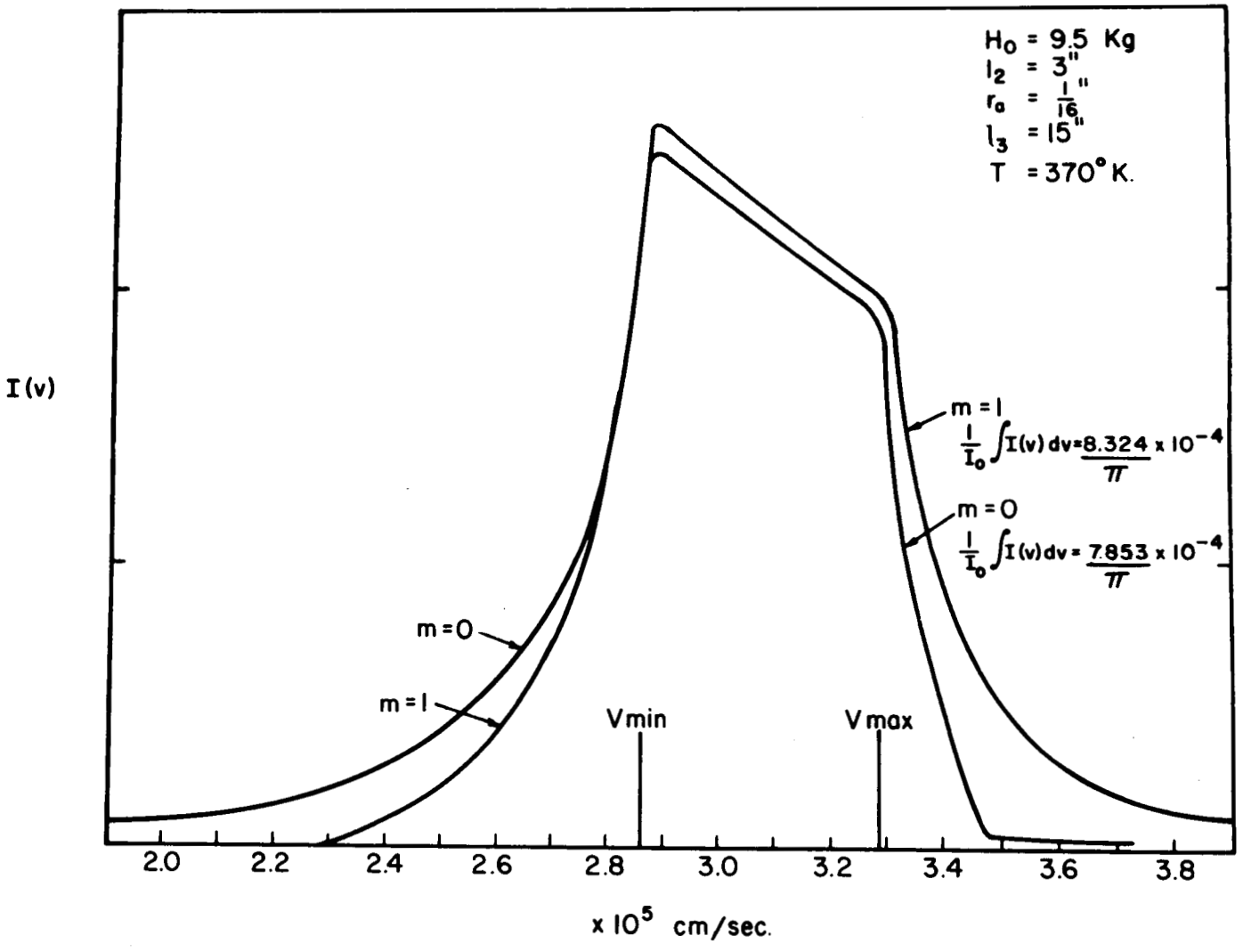

Fig. B-4. Intensity vs. Velocity curve, r.f. discharge source.

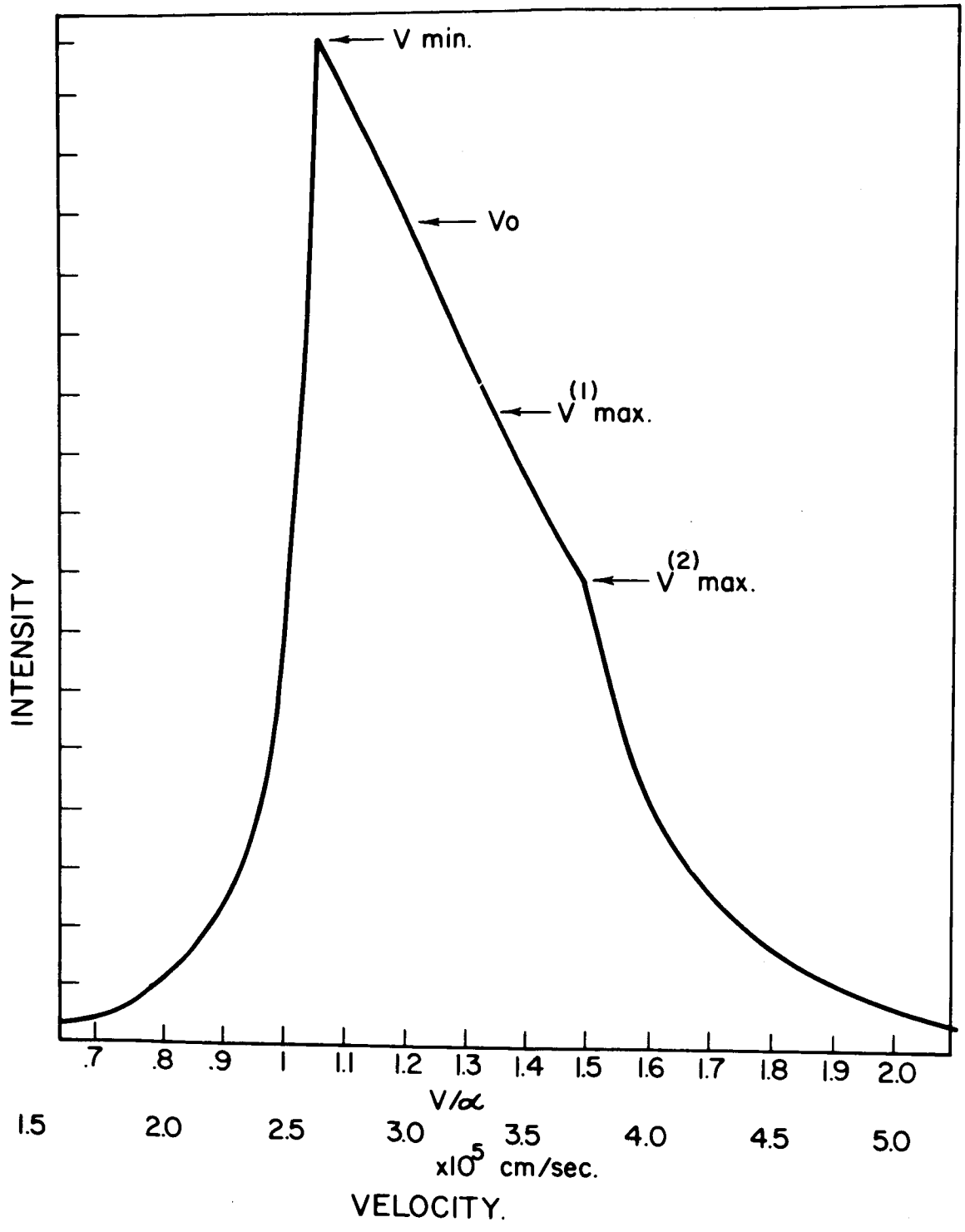

Fig. B-3. Theoretical Intensity vs. Velocity Curve.

VELOCITY	ANGLE(MIN)	ANGLE(MAX)	DELTA OMEGA	DELTA S	S
200000.0	0.224	0.542	0.2331092E-03	0.1006934E-05	0.7852638E-03
198000.0	0.226	0.536	0.2260581E-03	0.9596180E-06	
196000.0	0.226	0.528	0.2179123E-03	0.9086743E-06	
194000.0	0.228	0.522	0.2110144E-03	0.8639637E-06	
192000.0	0.228	0.516	0.2050543E-03	0.8239773E-06	
190000.0	0.230	0.510	0.1982865E-03	0.7816377E-06	
188000.0	0.230	0.504	0.1924643E-03	0.7439236E-06	
186000.0	0.232	0.498	0.1858266E-03	0.7039619E-06	
184000.0	0.234	0.492	0.1792503E-03	0.6652083E-06	
182000.0	0.236	0.486	0.1727351E-03	0.6276618E-06	
180000.0	0.236	0.480	0.1671885E-03	0.5944461E-06	
178000.0	0.238	0.474	0.1608035E-03	0.5593614E-06	
176000.0	0.240	0.470	0.1562751E-03	0.5314768E-06	
174000.0	0.242	0.464	0.1499896E-03	0.4984593E-06	
172000.0	0.244	0.460	0.1455224E-03	0.4723289E-06	
170000.0	0.246	0.454	0.1393365E-03	0.4414626E-06	
168000.0	0.250	0.450	0.1339774E-03	0.4141321E-06	
166000.0	0.252	0.446	0.1295868E-03	0.3905766E-06	
164000.0	0.256	0.440	0.1225549E-03	0.3599727E-06	
162000.0	0.260	0.436	0.1172264E-03	0.3353578E-06	
160000.0	0.264	0.432	0.1118980E-03	0.3115983E-06	
158000.0	0.270	0.428	0.1055398E-03	0.2859036E-06	
156000.0	0.276	0.424	0.9914329E-04	0.2611158E-06	
154000.0	0.284	0.420	0.9162527E-04	0.2344670E-06	
152000.0	0.294	0.414	0.8130517E-04	0.2020253E-06	
150000.0	0.310	0.400	0.6115114E-04	0.1474458E-06	
202000.0	0.224	0.550	0.2414694E-03	0.1060916E-05	
204000.0	0.222	0.556	0.2486735E-03	0.1110817E-05	
206000.0	0.222	0.564	0.2572481E-03	0.1167826E-05	
208000.0	0.222	0.572	0.2659451E-03	0.1226459E-05	
210000.0	0.220	0.582	0.2778346E-03	0.1301086E-05	
212000.0	0.220	0.590	0.2868073E-03	0.1363311E-05	
214000.0	0.220	0.598	0.2959024E-03	0.1427140E-05	
216000.0	0.218	0.608	0.3082819E-03	0.1508031E-05	
218000.0	0.218	0.618	0.3200145E-03	0.1587115E-05	
220000.0	0.218	0.628	0.3319385E-03	0.1668430E-05	
222000.0	0.216	0.638	0.3448845E-03	0.1756193E-05	
224000.0	0.216	0.650	0.3596756E-03	0.1854797E-05	
226000.0	0.216	0.660	0.3722121E-03	0.1943137E-05	
228000.0	0.216	0.672	0.3875085E-03	0.2047217E-05	
230000.0	0.214	0.686	0.4065256E-03	0.2172624E-05	
232000.0	0.214	0.698	0.4224191E-03	0.2282969E-05	
234000.0	0.214	0.712	0.4413099E-03	0.2411057E-05	
236000.0	0.214	0.728	0.4633588E-03	0.2558220E-05	
238000.0	0.214	0.744	0.4858976E-03	0.2710021E-05	
240000.0	0.212	0.760	0.5097417E-03	0.2871032E-05	
242000.0	0.212	0.778	0.5362348E-03	0.3048995E-05	
244000.0	0.212	0.796	0.5633480E-03	0.3232568E-05	
246000.0	0.212	0.816	0.5942010E-03	0.3439778E-05	
248000.0	0.212	0.836	0.6258196E-03	0.3653681E-05	
250000.0	0.210	0.860	0.6655803E-03	0.3917653E-05	
252000.0	0.210	0.884	0.7056357E-03	0.4186115E-05	
254000.0	0.210	0.910	0.7502731E-03	0.4484534E-05	
256000.0	0.210	0.938	0.7997911E-03	0.4815103E-05	
258000.0	0.210	0.968	0.8545112E-03	0.5180155E-05	
260000.0	0.210	1.002	0.9186098E-03	0.5605549E-05	
262000.0	0.210	1.038	0.9888902E-03	0.6072458E-05	
264000.0	0.208	1.078	0.1070689E-02	0.6614204E-05	
266000.0	0.208	1.122	0.1163324E-02	0.7227408E-05	
268000.0	0.208	1.170	0.1268607E-02	0.7924048E-05	
270000.0	0.208	1.224	0.1392321E-02	0.8741169E-05	
272000.0	0.208	1.282	0.1531416E-02	0.9660647E-05	
274000.0	0.208	1.350	0.1702691E-02	0.1078962E-04	
276000.0	0.208	1.424	0.1899135E-02	0.1208532E-04	
278000.0	0.208	1.510	0.2140503E-02	0.1367560E-04	
280000.0	0.206	1.608	0.2433813E-02	0.1560566E-04	
282000.0	0.206	1.720	0.2790512E-02	0.1795320E-04	
284000.0	0.206	1.852	0.3241730E-02	0.2092072E-04	
286000.0	0.206	2.006	0.3810300E-02	0.2465928E-04	
288000.0	0.206	2.018	0.3856510E-02	0.2502176E-04	
290000.0	0.206	2.004	0.3802625E-02	0.2472810E-04	
292000.0	0.206	1.990	0.3749114E-02	0.2442881E-04	
294000.0	0.206	1.974	0.3688419E-02	0.2407484E-04	
296000.0	0.206	1.960	0.3635713E-02	0.2376547E-04	
298000.0	0.206	1.948	0.3590835E-02	0.2350016E-04	
300000.0	0.206	1.934	0.3538825E-02	0.2318135E-04	
302000.0	0.204	1.920	0.3487975E-02	0.2286356E-04	
304000.0	0.204	1.908	0.3444016E-02	0.2258467E-04	
306000.0	0.204	1.896	0.3400332E-02	0.2230159E-04	
308000.0	0.204	1.882	0.3349715E-02	0.2196734E-04	
310000.0	0.204	1.870	0.3306628E-02	0.2167700E-04	
312000.0	0.204	1.856	0.3256709E-02	0.2133670E-04	
314000.0	0.204	1.844	0.3214219E-02	0.2104017E-04	
316000.0	0.204	1.832	0.3172005E-02	0.2074075E-04	
318000.0	0.204	1.822	0.3137037E-02	0.2048422E-04	
320000.0	0.204	1.810	0.3095328E-02	0.2017941E-04	
322000.0	0.204	1.798	0.3053895E-02	0.1987245E-04	
324000.0	0.204	1.786	0.3012737E-02	0.1956358E-04	
326000.0	0.204	1.774	0.2971855E-02	0.1925303E-04	
328000.0	0.204	1.764	0.2937998E-02	0.1898466E-04	
330000.0	0.202	1.594	0.2392476E-02	0.1541610E-04	
332000.0	0.202	1.424	0.1901490E-02	0.1221500E-04	
334000.0	0.202	1.278	0.1523970E-02	0.9757653E-05	
336000.0	0.202	1.148	0.1222159E-02	0.7797650E-05	
338000.0	0.202	1.030	0.9762122E-03	0.6205055E-05	
340000.0	0.202	0.918	0.7674222E-03	0.4858475E-05	
342000.0	0.202	0.810	0.5888266E-03	0.3712074E-05	
344000.0	0.202	0.686	0.4113029E-03	0.2581394E-05	
346000.0	0.202	0.330	0.6516665E-04	0.4070818E-06	
348000.0	0.202	0.314	0.5530591E-04	0.3437894E-06	
350000.0	0.202	0.304	0.4939177E-04	0.3054509E-06	
352000.0	0.202	0.296	0.4479826E-04	0.2755598E-06	
354000.0	0.202	0.290	0.4143351E-04	0.2514409E-06	
356000.0	0.202	0.286	0.3922862E-04	0.2385619E-06	
358000.0	0.202	0.280	0.3597871E-04	0.2174803E-06	
360000.0	0.202	0.276	0.3385039E-04	0.2033378E-06	
362000.0	0.202	0.274	0.3279771E-04	0.1957412E-06	
364000.0	0.202	0.270	0.3071531E-04	0.1820885E-06	
366000.0	0.202	0.268	0.2968560E-04	0.1747702E-06	
368000.0	0.202	0.266	0.2866355E-04	0.1675525E-06	
370000.0	0.200	0.262	0.2741181E-04	0.1590612E-06	
372000.0	0.200	0.260	0.2641272E-04	0.1521077E-06	
374000.0	0.200	0.258	0.2542128E-04	0.1452627E-06	
376000.0	0.200	0.256	0.2443751E-04	0.1385286E-06	
378000.0	0.200	0.256	0.2443751E-04	0.1373955E-06	
380000.0	0.200	0.254	0.2346139E-04	0.1308008E-06	

Fig. B-9(a). $T = 350^0$, $\ell_2 = 3''$, $m = 0$.

VELOCITY	ANGLE(MIN)	ANGLE(MAX)	DELTA OMEGA	DELTA S	S
240000.0	0.438	0.598	0.1586293E-03	0.8994520E-06	0.8324735E-03
238000.0	0.446	0.590	0.1315697E-03	0.7338104E-06	
236000.0	0.454	0.582	0.1032660E-03	0.5701351E-06	
234000.0	0.464	0.544	0.7717104E-04	0.4216171E-06	
232000.0	0.476	0.528	0.4996211E-04	0.2700708E-06	
230000.0	0.486	0.514	0.2679551E-04	0.1432051E-06	
228000.0	0.498	0.500	0.1910137E-05	0.1009130E-07	
242000.0	0.430	0.620	0.1909178E-03	0.1089546E-05	
244000.0	0.422	0.640	0.2215566E-03	0.1271372E-05	
246000.0	0.414	0.664	0.2579065E-03	0.1492998E-05	
248000.0	0.408	0.688	0.2936785E-03	0.1714563E-05	
250000.0	0.402	0.714	0.3321133E-03	0.1961317E-05	
252000.0	0.394	0.742	0.3783216E-03	0.2244356E-05	
254000.0	0.390	0.772	0.4247887E-03	0.2539049E-05	
256000.0	0.384	0.804	0.4774954E-03	0.2874738E-05	
258000.0	0.378	0.838	0.5352971E-03	0.3245039E-05	
260000.0	0.374	0.876	0.6005057E-03	0.3664412E-05	
262000.0	0.368	0.918	0.6768728E-03	0.4156459E-05	
264000.0	0.364	0.962	0.7588364E-03	0.4687728E-05	
266000.0	0.360	1.010	0.8521916E-03	0.5294428E-05	
268000.0	0.354	1.064	0.9634690E-03	0.6018078E-05	
270000.0	0.350	1.122	0.1087497E-02	0.6827445E-05	
272000.0	0.346	1.186	0.1236062E-02	0.7797664E-05	
274000.0	0.344	1.260	0.1406055E-02	0.8909895E-05	
276000.0	0.340	1.342	0.1612858E-02	0.1026356E-04	
278000.0	0.336	1.434	0.1859850E-02	0.1188196E-04	
280000.0	0.332	1.538	0.2158196E-02	0.1383840E-04	
282000.0	0.330	1.656	0.2520140E-02	0.1621377E-04	
284000.0	0.326	1.794	0.2978267E-02	0.1922044E-04	
286000.0	0.324	1.956	0.3560874E-02	0.2304506E-04	
288000.0	0.320	2.072	0.4010481E-02	0.2602076E-04	
290000.0	0.318	2.058	0.3956371E-02	0.2572790E-04	
292000.0	0.316	2.044	0.3902627E-02	0.2542908E-04	
294000.0	0.312	2.028	0.3842683E-02	0.2508174E-04	
296000.0	0.310	2.014	0.3789721E-02	0.2477216E-04	
298000.0	0.308	2.000	0.3737126E-02	0.2445756E-04	
300000.0	0.306	1.986	0.3684898E-02	0.2413821E-04	
302000.0	0.304	1.972	0.3633037E-02	0.2381444E-04	
304000.0	0.302	1.960	0.3589043E-02	0.2353571E-04	
306000.0	0.300	1.948	0.3545317E-02	0.2325250E-04	
308000.0	0.298	1.934	0.3494452E-02	0.2291652E-04	
310000.0	0.296	1.920	0.3443954E-02	0.2257726E-04	
312000.0	0.294	1.908	0.3401124E-02	0.2228285E-04	
314000.0	0.292	1.894	0.3351308E-02	0.2193754E-04	
316000.0	0.290	1.882	0.3309059E-02	0.2163691E-04	
318000.0	0.288	1.870	0.3267078E-02	0.2133336E-04	
320000.0	0.286	1.860	0.3232482E-02	0.2107356E-04	
322000.0	0.284	1.848	0.3190991E-02	0.2076457E-04	
324000.0	0.282	1.836	0.3149769E-02	0.2045341E-04	
326000.0	0.282	1.824	0.3107738E-02	0.2013334E-04	
328000.0	0.280	1.812	0.3067059E-02	0.1981862E-04	
330000.0	0.278	1.786	0.2978604E-02	0.1919287E-04	
332000.0	0.276	1.638	0.2494715E-02	0.1602582E-04	
334000.0	0.276	1.514	0.2120683E-02	0.1357828E-04	
336000.0	0.274	1.410	0.1830723E-02	0.1168043E-04	
338000.0	0.272	1.320	0.1596639E-02	0.1014865E-04	
340000.0	0.272	1.240	0.1400650E-02	0.8867381E-05	
342000.0	0.270	1.172	0.1244728E-02	0.7847001E-05	
344000.0	0.270	1.112	0.1113584E-02	0.6989009E-05	
346000.0	0.268	1.058	0.1002475E-02	0.6262244E-05	
348000.0	0.266	1.010	0.9085041E-03	0.5647390E-05	
350000.0	0.266	0.966	0.8253004E-03	0.5103863E-05	
352000.0	0.264	0.926	0.7538905E-03	0.4637277E-05	
354000.0	0.264	0.890	0.6913270E-03	0.4228716E-05	
356000.0	0.262	0.858	0.6388040E-03	0.3884773E-05	
358000.0	0.262	0.828	0.5903999E-03	0.3568787E-05	
360000.0	0.260	0.800	0.5477760E-03	0.3290466E-05	
362000.0	0.260	0.776	0.5115791E-03	0.3053173E-05	
364000.0	0.258	0.752	0.4774761E-03	0.2830605E-05	
366000.0	0.258	0.730	0.4462747E-03	0.2627386E-05	
368000.0	0.256	0.710	0.4196975E-03	0.2453338E-05	
370000.0	0.256	0.690	0.3929020E-03	0.2279873E-05	
372000.0	0.256	0.672	0.3694407E-03	0.2127566E-05	
374000.0	0.254	0.656	0.3500829E-03	0.2000450E-05	
376000.0	0.254	0.640	0.3302389E-03	0.1872021E-05	
378000.0	0.252	0.626	0.3142458E-03	0.1766791E-05	
380000.0	0.252	0.612	0.2976594E-03	0.1659497E-05	
382000.0	0.252	0.600	0.2837411E-03	0.1568298E-05	
384000.0	0.250	0.586	0.2688122E-03	0.1472697E-05	
386000.0	0.250	0.576	0.2576921E-03	0.1399048E-05	
388000.0	0.248	0.564	0.2455537E-03	0.1320854E-05	
390000.0	0.248	0.554	0.2348547E-03	0.1251394E-05	
392000.0	0.248	0.544	0.2243471E-03	0.1183891E-05	
394000.0	0.246	0.534	0.2149763E-03	0.1123282E-05	
396000.0	0.246	0.526	0.2068611E-03	0.1070028E-05	
398000.0	0.246	0.516	0.1968894E-03	0.1008017E-05	
400000.0	0.244	0.508	0.1899876E-03	0.9625235E-06	
402000.0	0.244	0.500	0.1822705E-03	0.9135976E-06	
404000.0	0.244	0.492	0.1746759E-03	0.8660364E-06	
406000.0	0.242	0.486	0.1699905E-03	0.8334988E-06	
408000.0	0.242	0.478	0.1626103E-03	0.7883483E-06	
410000.0	0.242	0.472	0.1571555E-03	0.7531868E-06	
412000.0	0.242	0.466	0.1517696E-03	0.7189097E-06	
414000.0	0.240	0.460	0.1473751E-03	0.6898328E-06	
416000.0	0.240	0.454	0.1421271E-03	0.6572649E-06	
418000.0	0.240	0.448	0.1369479E-03	0.6255721E-06	
420000.0	0.238	0.444	0.1344482E-03	0.6065271E-06	
422000.0	0.238	0.438	0.1293839E-03	0.5763193E-06	
424000.0	0.238	0.432	0.1243884E-03	0.5469731E-06	
426000.0	0.238	0.428	0.1210964E-03	0.5255762E-06	
428000.0	0.236	0.424	0.1187423E-03	0.5085619E-06	
430000.0	0.236	0.418	0.1139076E-03	0.4813281E-06	
432000.0	0.236	0.414	0.1107228E-03	0.4615213E-06	
434000.0	0.236	0.410	0.1075686E-03	0.4422043E-06	
436000.0	0.236	0.406	0.1044450E-03	0.4233745E-06	
438000.0	0.234	0.402	0.1012516E-03	0.4086238E-06	
440000.0	0.234	0.398	0.9918923E-04	0.3907077E-06	
442000.0	0.234	0.394	0.9615752E-04	0.3732690E-06	
444000.0	0.234	0.392	0.9465314E-04	0.3620284E-06	
446000.0	0.232	0.388	0.9255927E-04	0.3487502E-06	
448000.0	0.232	0.384	0.8960411E-04	0.3325276E-06	
450000.0	0.232	0.380	0.8667957E-04	0.3167672E-06	
452000.0	0.232	0.378	0.8522879E-04	0.3066564E-06	
454000.0	0.232	0.374	0.8250319E-04	0.2916698E-06	
456000.0	0.230	0.378	0.8180663E-04	0.2851646E-06	
458000.0	0.230	0.368	0.7897396E-04	0.2708886E-06	
460000.0	0.230	0.366	0.7756911E-04	0.2617670E-06	
462000.0	0.230	0.364	0.7617192E-04	0.2528483E-06	

Fig. B-9(b). $T = 370^0$, $\ell_2 = 3''$, $m = 1$.

VELOCITY	ANGLE(MIN)	ANGLE(MAX)	DELTA OMEGA	DELTA S	
600000.0	0.405	0.410	0.2670700E-03	0.1214511E-05	0.1824996E-03
595000.0	0.410	0.585	0.2355375E-03	0.1059689E-05	
590000.0	0.320	0.565	0.2074979E-03	0.9217666E-06	
585000.0	0.330	0.545	0.1800325E-03	0.7894186E-06	
580000.0	0.340	0.525	0.1531412E-03	0.6626077E-06	
575000.0	0.350	0.510	0.1316809E-03	0.5620200E-06	
570000.0	0.365	0.495	0.1069907E-03	0.4502928E-06	
565000.0	0.375	0.480	0.8591319E-04	0.3566436E-06	
560000.0	0.390	0.465	0.6136656E-04	0.2508874E-06	
555000.0	0.410	0.450	0.3292025E-04	0.1325821E-06	
605000.0	0.295	0.635	0.3025980E-03	0.1395060E-05	
610000.0	0.290	0.665	0.3427195E-03	0.1598697E-05	
615000.0	0.285	0.695	0.3845157E-03	0.1814297E-05	
620000.0	0.280	0.730	0.4349487E-03	0.2075232E-05	
625000.0	0.275	0.770	0.4950232E-03	0.2387578E-05	
630000.0	0.270	0.810	0.5581123E-03	0.2720366E-05	
635000.0	0.265	0.855	0.6323741E-03	0.3114047E-05	
640000.0	0.260	0.890	0.6933339E-03	0.3448356E-05	
645000.0	0.255	0.885	0.6873049E-03	0.3451528E-05	
650000.0	0.255	0.875	0.6704620E-03	0.3398632E-05	
655000.0	0.250	0.870	0.6645287E-03	0.3399290E-05	
660000.0	0.245	0.860	0.6503414E-03	0.3356126E-05	
665000.0	0.245	0.855	0.6421353E-03	0.3342141E-05	
670000.0	0.240	0.850	0.6362977E-03	0.3339181E-05	
675000.0	0.240	0.845	0.6281873E-03	0.3323007E-05	
680000.0	0.235	0.835	0.6143828E-03	0.3275110E-05	
685000.0	0.235	0.830	0.6064160E-03	0.3256759E-05	
690000.0	0.230	0.825	0.6007219E-03	0.3249382E-05	
695000.0	0.230	0.820	0.5928507E-03	0.3229017E-05	
700000.0	0.225	0.810	0.5794291E-03	0.3176941E-05	
705000.0	0.225	0.805	0.5717014E-03	0.3156437E-05	
710000.0	0.225	0.800	0.5640217E-03	0.3131376E-05	
715000.0	0.220	0.795	0.5585190E-03	0.3119076E-05	
720000.0	0.220	0.790	0.5509349E-03	0.3094046E-05	
725000.0	0.220	0.785	0.5433987E-03	0.3068135E-05	
730000.0	0.215	0.780	0.5379917E-03	0.3053181E-05	
735000.0	0.215	0.775	0.5305512E-03	0.3025645E-05	
740000.0	0.215	0.770	0.5231585E-03	0.2997304E-05	
745000.0	0.210	0.760	0.5105503E-03	0.2937905E-05	
750000.0	0.210	0.755	0.5033011E-03	0.2908195E-05	
755000.0	0.210	0.750	0.4960998E-03	0.2877776E-05	
760000.0	0.210	0.745	0.4889464E-03	0.2846676E-05	
765000.0	0.205	0.740	0.4838266E-03	0.2824524E-05	
770000.0	0.205	0.735	0.4767688E-03	0.2794184E-05	
775000.0	0.205	0.730	0.4697589E-03	0.2761244E-05	
780000.0	0.205	0.725	0.4627969E-03	0.2727740E-05	
785000.0	0.205	0.725	0.4627969E-03	0.2734549E-05	
790000.0	0.200	0.720	0.4578205E-03	0.2711279E-05	
795000.0	0.200	0.715	0.4509542E-03	0.2676063E-05	
800000.0	0.200	0.710	0.4441357E-03	0.2640383E-05	
805000.0	0.200	0.705	0.4371650E-03	0.2604266E-05	
810000.0	0.200	0.700	0.4306422E-03	0.2567742E-05	
815000.0	0.200	0.695	0.4239673E-03	0.2530841E-05	
820000.0	0.195	0.690	0.4192302E-03	0.2504882E-05	
825000.0	0.195	0.685	0.4126510E-03	0.2467318E-05	
830000.0	0.195	0.685	0.4126510E-03	0.2468531E-05	
835000.0	0.195	0.680	0.4061196E-03	0.2430130E-05	
840000.0	0.195	0.675	0.3996360E-03	0.2391482E-05	
845000.0	0.195	0.665	0.3868125E-03	0.2314395E-05	
850000.0	0.195	0.660	0.3555909E-03	0.2126817E-05	
855000.0	0.190	0.615	0.3274078E-03	0.1957130E-05	
860000.0	0.190	0.595	0.3042488E-03	0.1817272E-05	
865000.0	0.190	0.575	0.2818554E-03	0.1681951E-05	
870000.0	0.190	0.555	0.2602276E-03	0.1550939E-05	
875000.0	0.190	0.540	0.2445092E-03	0.1455216E-05	
880000.0	0.190	0.525	0.2292214E-03	0.1362039E-05	
885000.0	0.190	0.510	0.2143642E-03	0.1271453E-05	
890000.0	0.190	0.495	0.1999377E-03	0.1183501E-05	
895000.0	0.185	0.480	0.1877362E-03	0.1108819E-05	
900000.0	0.185	0.470	0.1786448E-03	0.1052579E-05	
905000.0	0.185	0.455	0.1653667E-03	0.9718007E-06	
910000.0	0.185	0.445	0.1567539E-03	0.9185999E-06	
915000.0	0.185	0.435	0.1483324E-03	0.8666377E-06	
920000.0	0.185	0.425	0.1401023E-03	0.8159342E-06	
925000.0	0.185	0.415	0.1320637E-03	0.7665079E-06	
930000.0	0.185	0.405	0.1242164E-03	0.7183752E-06	
935000.0	0.185	0.400	0.1203646E-03	0.6934675E-06	
940000.0	0.185	0.390	0.1128044E-03	0.6473291E-06	
945000.0	0.185	0.385	0.1090961E-03	0.6234431E-06	
950000.0	0.185	0.375	0.1018230E-03	0.5793477E-06	
955000.0	0.180	0.370	0.1000047E-03	0.5664184E-06	
960000.0	0.180	0.365	0.9648784E-04	0.5439145E-06	
965000.0	0.180	0.355	0.8959756E-04	0.5025902E-06	
970000.0	0.180	0.350	0.8622419E-04	0.4811998E-06	
975000.0	0.180	0.345	0.8289868E-04	0.4601946E-06	
980000.0	0.180	0.340	0.7962101E-04	0.4395808E-06	
985000.0	0.180	0.335	0.7639119E-04	0.4193640E-06	
990000.0	0.180	0.330	0.7320922E-04	0.3995496E-06	
995000.0	0.180	0.325	0.7007510E-04	0.3801422E-06	
1000000.0	0.180	0.320	0.6698883E-04	0.3611462E-06	
1005000.0	0.180	0.315	0.6395041E-04	0.3425654E-06	
1010000.0	0.180	0.310	0.6095984E-04	0.3244030E-06	
1015000.0	0.180	0.310	0.6095984E-04	0.3222164E-06	
1020000.0	0.180	0.305	0.5801711E-04	0.3045404E-06	
1025000.0	0.180	0.300	0.5512224E-04	0.2872915E-06	
1030000.0	0.180	0.295	0.5227521E-04	0.2704717E-06	
1035000.0	0.175	0.295	0.5397386E-04	0.2771804E-06	
1040000.0	0.175	0.290	0.5117468E-04	0.2608017E-06	
1045000.0	0.175	0.285	0.4842336E-04	0.2448556E-06	
1050000.0	0.175	0.285	0.4842336E-04	0.2429036E-06	
1055000.0	0.175	0.280	0.4571988E-04	0.2274742E-06	
1060000.0	0.175	0.280	0.4571988E-04	0.2255820E-06	
1065000.0	0.175	0.275	0.4306425E-04	0.2106753E-06	
1070000.0	0.175	0.275	0.4306425E-04	0.2088506E-06	
1075000.0	0.175	0.270	0.4045647E-04	0.1944708E-06	
1080000.0	0.175	0.270	0.4045647E-04	0.1927202E-06	
1085000.0	0.175	0.265	0.3789654E-04	0.1788701E-06	
1090000.0	0.175	0.265	0.3789654E-04	0.1771995E-06	
1095000.0	0.175	0.260	0.3538446E-04	0.1638803E-06	
1100000.0	0.175	0.260	0.3538446E-04	0.1622947E-06	
1105000.0	0.175	0.255	0.3292023E-04	0.1495062E-06	
1110000.0	0.175	0.255	0.3292023E-04	0.1480099E-06	
1115000.0	0.175	0.255	0.3292023E-04	0.1465040E-06	
1120000.0	0.175	0.250	0.3050385E-04	0.1343469E-06	
1125000.0	0.175	0.250	0.3050385E-04	0.1329357E-06	
1130000.0	0.175	0.245	0.2813531E-04	0.1213057E-06	
1135000.0	0.175	0.245	0.2813531E-04	0.1199917E-06	
1140000.0	0.175	0.245	0.2813531E-04	0.1186725E-06	

Fig. B-10. $T = 2800^0$, $\ell_2 = 8''$, $m = 0$.

VELOCITY	ANGLE(MIN)	ANGLE(MAX)	DELTA OMEGA	DELTA S	S
540000.0	0.290	0.446	0.1185088E-03	0.7231653E-06	0.5809451E-03
544000.0	0.296	0.450	0.1099419E-03	0.6664816E-06	
548000.0	0.302	0.446	0.1030784E-03	0.6205787E-06	
552000.0	0.312	0.442	0.9380335E-04	0.5606817E-06	
556000.0	0.322	0.438	0.8436753E-04	0.5005021E-06	
560000.0	0.338	0.434	0.7092383E-04	0.4174627E-06	
564000.0	0.360	0.430	0.5292109E-04	0.3089657E-06	
568000.0	0.284	0.460	0.1253110E-03	0.7694948E-06	
564000.0	0.280	0.464	0.1310069E-03	0.8092982E-06	
566000.0	0.276	0.470	0.1384982E-03	0.8604506E-06	
568000.0	0.272	0.474	0.1442095E-03	0.9007698E-06	
570000.0	0.268	0.480	0.1517543E-03	0.9527329E-06	
572000.0	0.266	0.484	0.1564665E-03	0.9870394E-06	
574000.0	0.262	0.490	0.1640802E-03	0.1039744E-05	
576000.0	0.260	0.496	0.1707408E-03	0.1088624E-05	
578000.0	0.258	0.502	0.1774526E-03	0.1133749E-05	
580000.0	0.256	0.508	0.1842457E-03	0.1181388E-05	
582000.0	0.254	0.514	0.1910900E-03	0.1229408E-05	
584000.0	0.252	0.520	0.1979955E-03	0.1277777E-05	
586000.0	0.250	0.528	0.2069798E-03	0.1339520E-05	
588000.0	0.248	0.534	0.2140308E-03	0.1388672E-05	
590000.0	0.246	0.542	0.2232140E-03	0.1451539E-05	
592000.0	0.244	0.548	0.2304105E-03	0.1501329E-05	
594000.0	0.242	0.556	0.2397927E-03	0.1565161E-05	
596000.0	0.242	0.564	0.2483673E-03	0.1623496E-05	
598000.0	0.240	0.572	0.2579868E-03	0.1688390E-05	
600000.0	0.238	0.582	0.2699453E-03	0.1768298E-05	
602000.0	0.238	0.590	0.2789179E-03	0.1828298E-05	
604000.0	0.236	0.600	0.2912132E-03	0.1909676E-05	
606000.0	0.236	0.610	0.3027927E-03	0.1985912E-05	
608000.0	0.234	0.620	0.3154631E-03	0.2068798E-05	
610000.0	0.234	0.632	0.3298408E-03	0.2162311E-05	
612000.0	0.232	0.642	0.3429246E-03	0.2246710E-05	
614000.0	0.232	0.654	0.3578076E-03	0.2342196E-05	
616000.0	0.230	0.666	0.3738504E-03	0.2444491E-05	
618000.0	0.230	0.680	0.3918838E-03	0.2558922E-05	
620000.0	0.228	0.694	0.4111689E-03	0.2680538E-05	
622000.0	0.228	0.708	0.4299525E-03	0.2797807E-05	
624000.0	0.228	0.724	0.4518788E-03	0.2934330E-05	
626000.0	0.226	0.740	0.4751641E-03	0.3078329E-05	
628000.0	0.226	0.758	0.5009681E-03	0.3237139E-05	
630000.0	0.226	0.776	0.5273923E-03	0.3398293E-05	
632000.0	0.224	0.794	0.5552978E-03	0.3567183E-05	
634000.0	0.224	0.816	0.5891941E-03	0.3772483E-05	
636000.0	0.224	0.838	0.6240167E-03	0.3981367E-05	
638000.0	0.222	0.860	0.6606193E-03	0.4199066E-05	
640000.0	0.222	0.886	0.7040624E-03	0.4457351E-05	
642000.0	0.222	0.912	0.7487994E-03	0.4720572E-05	
644000.0	0.220	0.942	0.8028726E-03	0.5038939E-05	
646000.0	0.220	0.972	0.8578224E-03	0.5358629E-05	
648000.0	0.220	1.006	0.9221812E-03	0.5732409E-05	
650000.0	0.220	1.042	0.9927372E-03	0.6139333E-05	
652000.0	0.218	1.080	0.1070742E-02	0.6586273E-05	
654000.0	0.218	1.122	0.1159247E-02	0.7090896E-05	
656000.0	0.218	1.168	0.1260055E-02	0.7662802E-05	
658000.0	0.218	1.220	0.1378889E-02	0.8334961E-05	
660000.0	0.216	1.274	0.1508601E-02	0.9062101E-05	
662000.0	0.216	1.336	0.1663459E-02	0.9927749E-05	
664000.0	0.216	1.402	0.1836392E-02	0.1088662E-04	
666000.0	0.216	1.478	0.2045855E-02	0.1204471E-04	
668000.0	0.216	1.560	0.2284253E-02	0.1335258E-04	
670000.0	0.214	1.572	0.2321043E-02	0.1346820E-04	
672000.0	0.214	1.564	0.2297034E-02	0.1322835E-04	
674000.0	0.214	1.554	0.2267196E-02	0.1295525E-04	
676000.0	0.214	1.546	0.2243463E-02	0.1271749E-04	
678000.0	0.214	1.538	0.2219853E-02	0.1248072E-04	
680000.0	0.212	1.530	0.2197180E-02	0.1224961E-04	
682000.0	0.212	1.522	0.2173814E-02	0.1201514E-04	
684000.0	0.212	1.514	0.2150571E-02	0.1178198E-04	
686000.0	0.212	1.506	0.2127451E-02	0.1155026E-04	
688000.0	0.212	1.498	0.2104453E-02	0.1132003E-04	
690000.0	0.212	1.490	0.2081577E-02	0.1109142E-04	
692000.0	0.210	1.480	0.2053963E-02	0.1083887E-04	
694000.0	0.210	1.472	0.2031363E-02	0.1061417E-04	
696000.0	0.210	1.466	0.2014493E-02	0.1042035E-04	
698000.0	0.210	1.458	0.1992138E-02	0.1019901E-04	
700000.0	0.210	1.450	0.1969844E-02	0.9979712E-05	
702000.0	0.210	1.442	0.1947704E-02	0.9767509E-05	
704000.0	0.210	1.436	0.1931179E-02	0.9574710E-05	
706000.0	0.210	1.428	0.1909253E-02	0.9361461E-05	
708000.0	0.208	1.422	0.1893688E-02	0.9180759E-05	
710000.0	0.208	1.414	0.1871976E-02	0.8971674E-05	
712000.0	0.208	1.406	0.1850387E-02	0.8765004E-05	
714000.0	0.208	1.400	0.1834275E-02	0.8585867E-05	
716000.0	0.208	1.392	0.1812900E-02	0.8383737E-05	
718000.0	0.208	1.386	0.1796950E-02	0.8208390E-05	
720000.0	0.208	1.378	0.1775789E-02	0.8010994E-05	
722000.0	0.208	1.372	0.1759999E-02	0.7839626E-05	
724000.0	0.206	1.366	0.1745070E-02	0.7673594E-05	
726000.0	0.206	1.360	0.1729418E-02	0.7505925E-05	
728000.0	0.206	1.354	0.1713834E-02	0.7340190E-05	
730000.0	0.206	1.346	0.1693164E-02	0.7154635E-05	
732000.0	0.206	1.340	0.1677741E-02	0.6993761E-05	
734000.0	0.206	1.334	0.1662387E-02	0.6833919E-05	
736000.0	0.206	1.326	0.1642023E-02	0.6656046E-05	
738000.0	0.206	1.312	0.1606680E-02	0.6420709E-05	
740000.0	0.206	1.234	0.1416636E-02	0.5580147E-05	
742000.0	0.206	1.164	0.1255998E-02	0.4875594E-05	
744000.0	0.204	1.100	0.1118120E-02	0.4276576E-05	
746000.0	0.204	1.042	0.9992296E-03	0.3764955E-05	
748000.0	0.204	0.990	0.8981113E-03	0.3332958E-05	
750000.0	0.204	0.940	0.8057627E-03	0.2944628E-05	
752000.0	0.204	0.896	0.7284539E-03	0.2621004E-05	
754000.0	0.204	0.854	0.6581159E-03	0.2330930E-05	
756000.0	0.204	0.816	0.5973859E-03	0.2083390E-05	
758000.0	0.204	0.780	0.5424016E-03	0.1860492E-05	
760000.0	0.204	0.746	0.4927496E-03	0.1662847E-05	
762000.0	0.204	0.714	0.4480394E-03	0.1487741E-05	
764000.0	0.204	0.686	0.4105258E-03	0.1340184E-05	
766000.0	0.204	0.658	0.3745127E-03	0.1202181E-05	
768000.0	0.202	0.632	0.3431926E-03	0.1083031E-05	
770000.0	0.202	0.606	0.3123893E-03	0.9689900E-06	
772000.0	0.202	0.584	0.2873356E-03	0.8758980E-06	
774000.0	0.202	0.562	0.2632082E-03	0.7883618E-06	
776000.0	0.202	0.542	0.2420760E-03	0.7123031E-06	
778000.0	0.202	0.522	0.2217134E-03	0.6407760E-06	
780000.0	0.202	0.504	0.2040399E-03	0.5791028E-06	
782000.0	0.202	0.486	0.1869865E-03	0.5210734E-06	

Fig. B - 11. $T = 370^0$, $\ell_2 = 4''$, $m = 0$.

VELOCITY	ANGLE(MIN)	ANGLE(MAX)	DELTA OMEGA	DELTA S	S
600000.0	0.305	0.610	0.2670700E-03	0.1214511E-05	0.1824996E-03
595000.0	0.310	0.585	0.2355375E-03	0.1059689E-05	
590000.0	0.320	0.565	0.2074979E-03	0.9217666E-06	
585000.0	0.330	0.545	0.1800325E-03	0.7894186E-06	
580000.0	0.340	0.525	0.1531412E-03	0.6626077E-06	
575000.0	0.350	0.510	0.1316809E-03	0.5620200E-06	
570000.0	0.365	0.495	0.1069907E-03	0.4502982E-06	
565000.0	0.375	0.480	0.8591319E-04	0.3564636E-06	
560000.0	0.390	0.465	0.6136656E-04	0.2508874E-06	
555000.0	0.410	0.450	0.3792025E-04	0.1325821E-06	
605000.0	0.295	0.635	0.3025980E-03	0.1395060E-05	
610000.0	0.290	0.665	0.3427195E-03	0.1598697E-05	
615000.0	0.285	0.695	0.3845157E-03	0.1814297E-05	
620000.0	0.280	0.730	0.4349487E-03	0.2075232E-05	
625000.0	0.275	0.770	0.4950232E-03	0.2387578E-05	
630000.0	0.270	0.810	0.5581123E-03	0.2720366E-05	
635000.0	0.265	0.855	0.6323741E-03	0.3114047E-05	
640000.0	0.260	0.890	0.6933339E-03	0.3448354E-05	
645000.0	0.255	0.885	0.6873049E-03	0.3451528E-05	
650000.0	0.255	0.875	0.6704620E-03	0.3398632E-05	
655000.0	0.250	0.870	0.6645287E-03	0.3399290E-05	
660000.0	0.245	0.860	0.6503414E-03	0.3356126E-05	
665000.0	0.245	0.855	0.6421353E-03	0.3342141E-05	
670000.0	0.240	0.850	0.6362977E-03	0.3339181E-05	
675000.0	0.240	0.845	0.6281873E-03	0.3323007E-05	
680000.0	0.235	0.835	0.6143828E-03	0.3275110E-05	
685000.0	0.235	0.830	0.6064160E-03	0.3256759E-05	
690000.0	0.230	0.825	0.6007219E-03	0.3249382E-05	
695000.0	0.230	0.820	0.5928507E-03	0.3229017E-05	
700000.0	0.225	0.810	0.5794291E-03	0.3176941E-05	
705000.0	0.225	0.805	0.5717014E-03	0.3154637E-05	
710000.0	0.225	0.800	0.5640217E-03	0.3131376E-05	
715000.0	0.220	0.795	0.5585190E-03	0.3119076E-05	
720000.0	0.220	0.790	0.5509349E-03	0.3094046E-05	
725000.0	0.220	0.785	0.5433987E-03	0.3068135E-05	
730000.0	0.215	0.780	0.5379917E-03	0.3053181E-05	
735000.0	0.215	0.775	0.5305512E-03	0.3025645E-05	
740000.0	0.215	0.770	0.5231585E-03	0.2997306E-05	
745000.0	0.210	0.760	0.5105503E-03	0.2937905E-05	
750000.0	0.210	0.755	0.5033011E-03	0.2909195E-05	
755000.0	0.210	0.750	0.4960998E-03	0.2877776E-05	
760000.0	0.210	0.745	0.4883464E-03	0.2846676E-05	
765000.0	0.205	0.740	0.4838266E-03	0.2826524E-05	
770000.0	0.205	0.735	0.4767688E-03	0.2794184E-05	
775000.0	0.205	0.730	0.4697589E-03	0.2761244E-05	
780000.0	0.205	0.725	0.4627969E-03	0.2727740E-05	
785000.0	0.205	0.725	0.4627969E-03	0.2734549E-05	
790000.0	0.200	0.720	0.4578205E-03	0.2711279E-05	
795000.0	0.200	0.715	0.4509542E-03	0.2676063E-05	
800000.0	0.200	0.710	0.4441357E-03	0.2640383E-05	
805000.0	0.200	0.705	0.4373650E-03	0.2604266E-05	
810000.0	0.200	0.700	0.4306422E-03	0.2567742E-05	
815000.0	0.200	0.695	0.4239673E-03	0.2530841E-05	
820000.0	0.195	0.690	0.4192302E-03	0.2504882E-05	
825000.0	0.195	0.685	0.4126510E-03	0.2466731E-05	
830000.0	0.195	0.685	0.4126510E-03	0.2468531E-05	
835000.0	0.195	0.680	0.4061196E-03	0.2430130E-05	
840000.0	0.195	0.675	0.3996360E-03	0.2391482E-05	
845000.0	0.195	0.665	0.3868125E-03	0.2314395E-05	
850000.0	0.195	0.660	0.3555909E-03	0.2126817E-05	
855000.0	0.190	0.615	0.3274078E-03	0.1957130E-05	
860000.0	0.190	0.595	0.3042488E-03	0.1817772E-05	
865000.0	0.190	0.575	0.2818554E-03	0.1681951E-05	
870000.0	0.190	0.555	0.2602276E-03	0.1550039E-05	
875000.0	0.190	0.540	0.2445092E-03	0.1455216E-05	
880000.0	0.190	0.525	0.2292214E-03	0.1362039E-05	
885000.0	0.190	0.510	0.2143642E-03	0.1271453E-05	
890000.0	0.190	0.495	0.1999377E-03	0.1183501E-05	
895000.0	0.185	0.480	0.1877362E-03	0.1108819E-05	
900000.0	0.185	0.470	0.1786448E-03	0.1052579E-05	
905000.0	0.185	0.455	0.1653667E-03	0.9718007E-06	
910000.0	0.185	0.445	0.1567539E-03	0.9185999E-06	
915000.0	0.185	0.435	0.1483324E-03	0.8665377E-06	
920000.0	0.185	0.425	0.1401023E-03	0.8159342E-06	
925000.0	0.185	0.415	0.1320637E-03	0.7665079E-06	
930000.0	0.185	0.405	0.1242164E-03	0.7183752E-06	
935000.0	0.185	0.400	0.1203646E-03	0.6934675E-06	
940000.0	0.185	0.390	0.1128044E-03	0.6473291E-06	
945000.0	0.185	0.385	0.1090961E-03	0.6234431E-06	
950000.0	0.185	0.375	0.1018230E-03	0.5793477E-06	
955000.0	0.180	0.370	0.1000047E-03	0.5664184E-06	
960000.0	0.180	0.365	0.9648784E-04	0.5439145E-06	
965000.0	0.180	0.355	0.8959756E-04	0.5025902E-06	
970000.0	0.180	0.350	0.8622419E-04	0.4811998E-06	
975000.0	0.180	0.345	0.8289868E-04	0.4601946E-06	
980000.0	0.180	0.340	0.7962101E-04	0.4395808E-06	
985000.0	0.180	0.335	0.7639119E-04	0.4193640E-06	
990000.0	0.180	0.330	0.7320922E-04	0.3995496E-06	
995000.0	0.180	0.325	0.7007510E-04	0.3801422E-06	
1000000.0	0.180	0.320	0.6698883E-04	0.3611462E-06	
1005000.0	0.180	0.315	0.6395041E-04	0.3425656E-06	
1010000.0	0.180	0.310	0.6095984E-04	0.3244030E-06	
1015000.0	0.180	0.310	0.6095984E-04	0.3222164E-06	
1020000.0	0.180	0.305	0.5801711E-04	0.3044404E-06	
1025000.0	0.180	0.300	0.5512224E-04	0.2872915E-06	
1030000.0	0.180	0.295	0.5227521E-04	0.2704717E-06	
1035000.0	0.175	0.295	0.5397386E-04	0.2771804E-06	
1040000.0	0.175	0.290	0.5117468E-04	0.2608017E-06	
1045000.0	0.175	0.285	0.4842336E-04	0.2448656E-06	
1050000.0	0.175	0.285	0.4842336E-04	0.2429036E-06	
1055000.0	0.175	0.280	0.4571988E-04	0.2274742E-06	
1060000.0	0.175	0.280	0.4571988E-04	0.2255820E-06	
1065000.0	0.175	0.275	0.4306425E-04	0.2106753E-06	
1070000.0	0.175	0.275	0.4306425E-04	0.2088506E-06	
1075000.0	0.175	0.270	0.4045647E-04	0.1944708E-06	
1080000.0	0.175	0.270	0.4045647E-04	0.1927202E-06	
1085000.0	0.175	0.265	0.3789654E-04	0.1784701E-06	
1090000.0	0.175	0.265	0.3789654E-04	0.1771995E-06	
1095000.0	0.175	0.260	0.3538446E-04	0.1638803E-06	
1100000.0	0.175	0.260	0.3538446E-04	0.1622947E-06	
1105000.0	0.175	0.255	0.3292023E-04	0.1495062E-06	
1110000.0	0.175	0.255	0.3292023E-04	0.1480099E-06	
1115000.0	0.175	0.255	0.3292023E-04	0.1465040E-06	
1120000.0	0.175	0.250	0.3050385E-04	0.1343469E-06	
1125000.0	0.175	0.250	0.3050385E-04	0.1329357E-06	
1130000.0	0.175	0.245	0.2813531E-04	0.1213057E-06	
1135000.0	0.175	0.245	0.2813531E-04	0.1199917E-06	
1140000.0	0.175	0.245	0.2813531E-04	0.1186725E-06	

Fig. B-12. $T = 2800^0$, $\ell_2 = 6.25''$, $m = 0$.

VELOCITY	ANGLE(MIN)	ANGLE(MAX)	DELTA OMEGA	DELTA S	S
640000.0	0.400	0.480	0.6737162E-04	0.3476753E-06	0.1640845E-03
655000.0	0.410	0.465	0.4605484E-04	0.2355862E-06	
650000.0	0.425	0.455	0.2526437E-04	0.1280674E-06	
665000.0	0.385	0.495	0.9263599E-04	0.4821453E-06	
670000.0	0.375	0.510	0.1143356E-03	0.6000136E-06	
675000.0	0.365	0.525	0.1362744E-03	0.7208492E-06	
680000.0	0.355	0.545	0.1636441E-03	0.8723431E-06	
685000.0	0.345	0.565	0.1915880E-03	0.1028924E-05	
690000.0	0.335	0.585	0.2201061E-03	0.1190582E-05	
695000.0	0.330	0.605	0.2460642E-03	0.1340212E-05	
700000.0	0.320	0.630	0.2818315E-03	0.1545249E-05	
705000.0	0.315	0.655	0.3156130E-03	0.1741546E-05	
710000.0	0.310	0.685	0.3570742E-03	0.1982430E-05	
715000.0	0.300	0.715	0.4031050E-03	0.2251159E-05	
720000.0	0.295	0.745	0.4478679E-03	0.2515222E-05	
725000.0	0.290	0.785	0.5092344E-03	0.2875236E-05	
730000.0	0.285	0.780	0.5044973E-03	0.2863095E-05	
735000.0	0.280	0.775	0.4997603E-03	0.2850050E-05	
740000.0	0.275	0.770	0.4950232E-03	0.2836112E-05	
745000.0	0.275	0.765	0.4876784E-03	0.2804291E-05	
750000.0	0.270	0.760	0.4829892E-03	0.2790828E-05	
755000.0	0.265	0.755	0.4783000E-03	0.2774523E-05	
760000.0	0.260	0.750	0.4736108E-03	0.2757391E-05	
765000.0	0.260	0.745	0.4664573E-03	0.2725052E-05	
770000.0	0.255	0.740	0.4618160E-03	0.2706550E-05	
775000.0	0.250	0.735	0.4571746E-03	0.2687276E-05	
780000.0	0.250	0.730	0.4501647E-03	0.2653286E-05	
785000.0	0.245	0.725	0.4455712E-03	0.2632767E-05	
790000.0	0.245	0.720	0.4386570E-03	0.2597789E-05	
795000.0	0.240	0.715	0.4341113E-03	0.2576114E-05	
800000.0	0.240	0.710	0.4272928E-03	0.2540252E-05	
805000.0	0.235	0.705	0.4227950E-03	0.2517509E-05	
810000.0	0.235	0.700	0.4160722E-03	0.2480867E-05	
815000.0	0.230	0.695	0.4116222E-03	0.2457148E-05	
820000.0	0.230	0.695	0.4116222E-03	0.2459425E-05	
825000.0	0.225	0.690	0.4071723E-03	0.2434560E-05	
830000.0	0.225	0.685	0.4005930E-03	0.2396399E-05	
835000.0	0.225	0.680	0.3940616E-03	0.2357978E-05	
840000.0	0.220	0.675	0.3897073E-03	0.2332068E-05	
845000.0	0.220	0.670	0.3832716E-03	0.2293209E-05	
850000.0	0.220	0.670	0.3832716E-03	0.2292378E-05	
855000.0	0.215	0.665	0.3789652E-03	0.2265323E-05	
860000.0	0.215	0.660	0.3726252E-03	0.2225683E-05	
865000.0	0.215	0.655	0.3663330E-03	0.2185935E-05	
870000.0	0.215	0.650	0.3600887E-03	0.2146105E-05	
875000.0	0.210	0.650	0.3621223E-03	0.2155200E-05	
880000.0	0.210	0.645	0.3559259E-03	0.2114920E-05	
885000.0	0.210	0.640	0.3497773E-03	0.2074625E-05	
890000.0	0.210	0.635	0.3436765E-03	0.2034341E-05	
895000.0	0.205	0.635	0.3456622E-03	0.2041571E-05	
900000.0	0.205	0.630	0.3396033E-03	0.2000984E-05	
905000.0	0.205	0.625	0.3336043E-03	0.1960472E-05	
910000.0	0.205	0.625	0.3336043E-03	0.1956496E-05	
915000.0	0.205	0.620	0.3276470E-03	0.1914290E-05	
920000.0	0.200	0.615	0.3236755E-03	0.1885036E-05	
925000.0	0.200	0.615	0.3236755E-03	0.1874638E-05	
930000.0	0.200	0.610	0.3178140E-03	0.1837999E-05	
935000.0	0.200	0.605	0.3120004E-03	0.1797557E-05	
940000.0	0.200	0.605	0.3120004E-03	0.1790417E-05	
945000.0	0.195	0.600	0.3081246E-03	0.1760816E-05	
950000.0	0.195	0.595	0.3024366E-03	0.1720619E-05	
955000.0	0.195	0.595	0.3024366E-03	0.1713905E-05	
960000.0	0.195	0.590	0.2967365E-03	0.1677242E-05	
965000.0	0.195	0.585	0.2911142E-03	0.1632981E-05	
970000.0	0.195	0.585	0.2911142E-03	0.1624450E-05	
975000.0	0.195	0.580	0.2855398E-03	0.1585114E-05	
980000.0	0.190	0.580	0.2873820E-03	0.1586511E-05	
985000.0	0.190	0.575	0.2818554E-03	0.1547299E-05	
990000.0	0.190	0.570	0.2763767E-03	0.1503365E-05	
995000.0	0.190	0.565	0.2602276E-03	0.1411678E-05	
1000000.0	0.190	0.560	0.2445092E-03	0.1318184E-05	
1005000.0	0.190	0.525	0.2292214E-03	0.1227878E-05	
1010000.0	0.190	0.510	0.2143642E-03	0.1140758E-05	
1015000.0	0.185	0.500	0.2064930E-03	0.1091466E-05	
1020000.0	0.185	0.485	0.1923536E-03	0.1009692E-05	
1025000.0	0.185	0.475	0.1831666E-03	0.9544458E-06	
1030000.0	0.185	0.465	0.1741709E-03	0.9011595E-06	
1035000.0	0.185	0.455	0.1653667E-03	0.8492333E-06	
1040000.0	0.185	0.445	0.1567539E-03	0.7986652E-06	
1045000.0	0.185	0.435	0.1483324E-03	0.7500518E-06	
1050000.0	0.185	0.425	0.1401023E-03	0.7037881E-06	
1055000.0	0.185	0.420	0.1360591E-03	0.6769469E-06	
1060000.0	0.185	0.410	0.1281161E-03	0.6321255E-06	
1065000.0	0.180	0.400	0.1221111E-03	0.5973914E-06	
1070000.0	0.180	0.395	0.1183071E-03	0.5737590E-06	
1075000.0	0.180	0.390	0.1145509E-03	0.5504362E-06	
1080000.0	0.180	0.380	0.1071821E-03	0.5105775E-06	
1085000.0	0.180	0.375	0.1035695E-03	0.4888437E-06	
1090000.0	0.180	0.370	0.1000047E-03	0.4676098E-06	
1095000.0	0.180	0.365	0.9644784E-04	0.4468756E-06	
1100000.0	0.180	0.360	0.9301877E-04	0.4264408E-06	
1105000.0	0.180	0.350	0.8622419E-04	0.3915845E-06	
1110000.0	0.180	0.345	0.8289868E-04	0.3727138E-06	
1115000.0	0.180	0.340	0.7962101E-04	0.3543353E-06	
1120000.0	0.180	0.340	0.7962101E-04	0.3504717E-06	
1125000.0	0.180	0.335	0.7639119E-04	0.3327128E-06	
1130000.0	0.175	0.330	0.7490787E-04	0.3229660E-06	
1135000.0	0.175	0.325	0.7177375E-04	0.3061014E-06	
1140000.0	0.175	0.320	0.6869748E-04	0.2897183E-06	
1145000.0	0.175	0.315	0.6564905E-04	0.2738131E-06	
1150000.0	0.175	0.315	0.6564905E-04	0.2707139E-06	
1155000.0	0.175	0.310	0.6265848E-04	0.2554156E-06	
1160000.0	0.175	0.305	0.5971576E-04	0.2405844E-06	
1165000.0	0.175	0.300	0.5682089E-04	0.2262218E-06	
1170000.0	0.175	0.300	0.5682089E-04	0.2235158E-06	
1175000.0	0.175	0.295	0.5397386E-04	0.2097431E-06	
1180000.0	0.175	0.290	0.5117468E-04	0.1964236E-06	
1185000.0	0.175	0.290	0.5117468E-04	0.1939803E-06	
1190000.0	0.175	0.285	0.4842336E-04	0.1812392E-06	
1195000.0	0.175	0.285	0.4842336E-04	0.1789278E-06	
1200000.0	0.175	0.280	0.4571988E-04	0.1667571E-06	
1205000.0	0.175	0.280	0.4571988E-04	0.1645781E-06	
1210000.0	0.170	0.275	0.4471505E-04	0.1588326E-06	
1215000.0	0.170	0.275	0.4471505E-04	0.1567075E-06	
1220000.0	0.170	0.270	0.4210727E-04	0.1455711E-06	
1225000.0	0.170	0.270	0.4210727E-04	0.1435786E-06	
1230000.0	0.170	0.265	0.3954734E-04	0.1329827E-06	
1235000.0	0.170	0.265	0.3954734E-04	0.1311213E-06	

Fig. B-13. $T = 2800^0$, $\ell_2 = 9.375"$, $m = 0.$

C. AUTOMATIC TUNING SYSTEM*

Background

The oscillation frequency of a hydrogen maser is "pulled" by the maser cavity resonator. The degree of pulling depends on the cavity detuning and the atomic resonance linewidth in the following way:[6]

$$\nu = \nu_H + \left[\frac{\nu_c - \nu_H}{\nu_c} Q - \frac{0.29 \bar{v} a_0^2 \hbar V_c}{Q \mu_0^2 \eta V_b} \right] \Delta\nu_\ell \qquad (1)$$

where
- ν = Maser oscillation frequency
- ν_H = Atomic resonance frequency
- ν_c = Cavity center frequency
- Q = Quality factor of cavity
- $\bar{v}$ = Mean velocity of the hydrogen atom
- a_0 = First Bohr orbit radius
- $\hbar$ = Planck's constant divided by 2π
- μ_0 = Bohr magneton
- V_c = Volume of cavity
- V_b = Volume of storage bulb
- η = Ratio of average electromagnetic field energy density in the bulb to average energy density taken over the cavity
- $\Delta\nu_\ell$ = Atomic resonance linewidth

It is apparent that if the cavity is tuned to

$$\nu_{c_0} = \nu_H \left[\frac{I}{1 - \frac{0.29 \bar{v} a_0^2 \hbar V_c}{Q^2 \mu_0^2 \eta V_b}} \right] \qquad (2)$$

then the term in the brackets in equation (1) vanishes and

$$\nu = \nu_H \qquad (3)$$

that is, the maser oscillates at exactly the center of the atomic resonance line.

*The work described in this section was performed in part under Contract NASW-1337 and will be reported to NASA under that contract.

The cavity can be tuned to ν_c by making use of the fact that the linewidth $\Delta\nu$ is proportional to I_{tot}, the total flux of atoms entering the bulb. It can be shown[2] that

$$\Delta\nu_{S.E.} = \frac{1}{\pi\sqrt{2}} \frac{T_b}{V_b} \sigma \bar{v} I_{tot} \tag{4}$$

where $\Delta\nu_{S.E.}$ is the spin exchange contribution to the linewidth and T_b is the mean storage time of the bulb. It can be seen from equation (1) that at the correct cavity tuning point, ν_{c_0}, ν is independent of I_{tot}, the total hydrogen flux. The criterion for correct cavity tuning is that no shift in maser oscillation frequency results from a change in the flux of atomic hydrogen.

Detailed System Analysis

The automatic tuner exploits the physical phenomena described in the previous section. The system is capable of retuning an initially detuned maser and of holding this tuned condition indefinitely.

Operation of the Automatic Tuner

The automatic tuner operates on the beat between the controlled maser and a reference maser. The reference maser is offset in frequency, either by increasing the C field or by offsetting the synthesizer in the phase lock loop of one of the masers as will be described in a later section. This offset, in the order of 1 in 10^{-11}, eliminates the necessity for determining if the controlled maser is higher or lower in frequency than the reference and also avoids the possibility of excessively long beats.

The low frequency beat is fed into the input of the period gate generator as shown in the block diagram, Fig. C-1. The period gate generator produces a gating signal which begins at the first positive-going zero crossing of the beat input after an enabling pulse from the master timer and which ends after 1, 10, 100 or 1000 periods of the input as selected by a switch. This gating pulse closes the master gate, also located in the period gate generator, allowing the reversible counter to accumulate a 10 Hz pulse stream supplied from the master timer.

The digital-to-analog converter produces on command an analog voltage proportional to the digital reading in the register of the reversible counter. This analog voltage is amplified and processed in the varactor voltage controller and then supplied to the varactor tuner in the maser cavity. The register of the reversible counter is not reset, the cycle repeats and the tuning continues until there is no further change in the counter register.

The pressure control provides for the presetting of two hydrogen pressure levels in the maser and for switching between these two pressures under control of the master timer.

The time sequence of the tuning cycle is as follows:

a) An initial command from the master timer at time t = 0 sets the pressure of the controlled maser to a low level and also sets the reversible counter to read "up."

b) At t = 240 seconds, allowing the controlled maser pressure time to stabilize, the master timer enables the period gate generator, starting the period measuring process. The reversible counter measures the period (or a multiple of the period) of the beat, counting up on the 10 kHz pulse stream from the master gate.

c) At t = 700 seconds, a command from the master timer sets the pressure of the controlled maser to a relatively high flux level and sets the counter to count down.

d) At t = 942 seconds, the period gate generator is again "enabled" and the counter again digitally measures the beat period (or a multiple thereof), this time counting downwards. The number remaining in the counter register is a measure of the change in frequency of the controlled maser resulting from the change in hydrogen flux. As can be seen from Fig. C-2, if the reference maser is offset to a frequency higher than the controlled maser, the residue in the register will be positive if the controlled maser frequency goes down with increasing flux (and negative if the maser frequency goes up with increasing flux). An electrical signal indicating the sign of residue in the register is fed to the varactor voltage controller.

e) At t = 1410 seconds a command from the master timer transfers the binary-coded digital residue in the counter register to the register in the D-A converter. The converter produces an analog voltage proportional to the digital residue which is amplified and processed in the varactor voltage controller. The magnitude and sign of the gain of the varactor voltage controller is adjusted for negative feedback; in the situation illustrated in Fig. C-2, the change in voltage should be such as to raise the frequency of the maser cavity frequency as shown by the dotted lines.

Note that the magnitude of the analog voltage is proportional to the numerical value of the residue in the counter; the sign of the correction depends on the sign signal from the counter register.

f) At t = 1500 seconds, a master timer reset pulse sets the timer back to zero and the cycle repeats from step (a); the varactor voltage is automatically re-adjusted on each cycle until there is no further change in the counter residue. It should be noted that this system is a true integrating digital servo; there is no possibility of a steady-state error except for the granularity of the digital-to-analog conversion.

Period Gate Generator

Fig. C-3 is a circuit diagram of the period gate generator. The beat input is fed to Q1, an integrated circuit operational amplifier. The amplifier stage is d.c. coupled and carefully designed to minimize drift and high-frequency noise. Q2 is also an integrated operational amplifier, arranged as a Schmitt trigger.

The square-wave output from the Schmitt trigger stage is one input to the number 1 nand gate of the integrated dual two-input nand gate, Q3. The gate is normally held open by a logic signal from the output of the integrated J-K flip-flop, Q8. The negative-going transition of the enable pulse triggers Q8, which in turn closes gate 1 of Q3. In the one position of the period average switch, the square-wave output of Q2 is transmitted directly to the integrated J-K flip-flop, Q12. Since the J-K flip-flop changes state only on negative transitions, the output of Q12 is a pulse, the length of which is equal to one period of the input beat signal. This period pulse serves two functions: it opens gate 1 of the dual nand gate Q13 to permit the pulse stream from the "pulse input" jack to appear at the "gated pulse out" jack; the trailing edge of the gating pulse retriggers the J-K flip-flop Q8 through gate 2 of Q3, thus opening gate 1 of Q3 and terminating the period measuring process until another enable pulse is received.

In the 10, 100 and 1000 positions of the period average switch, integrated decade counters Q5, Q6 and Q7 are successively switched into the circuit. Since each decade counter produces an output pulse only after ten input pulses, the length of the gating signal applied to gate 1 of Q13 is equal in length to 1, 10, 100 or 1000 periods of the beat input, as selected by the period average switch.

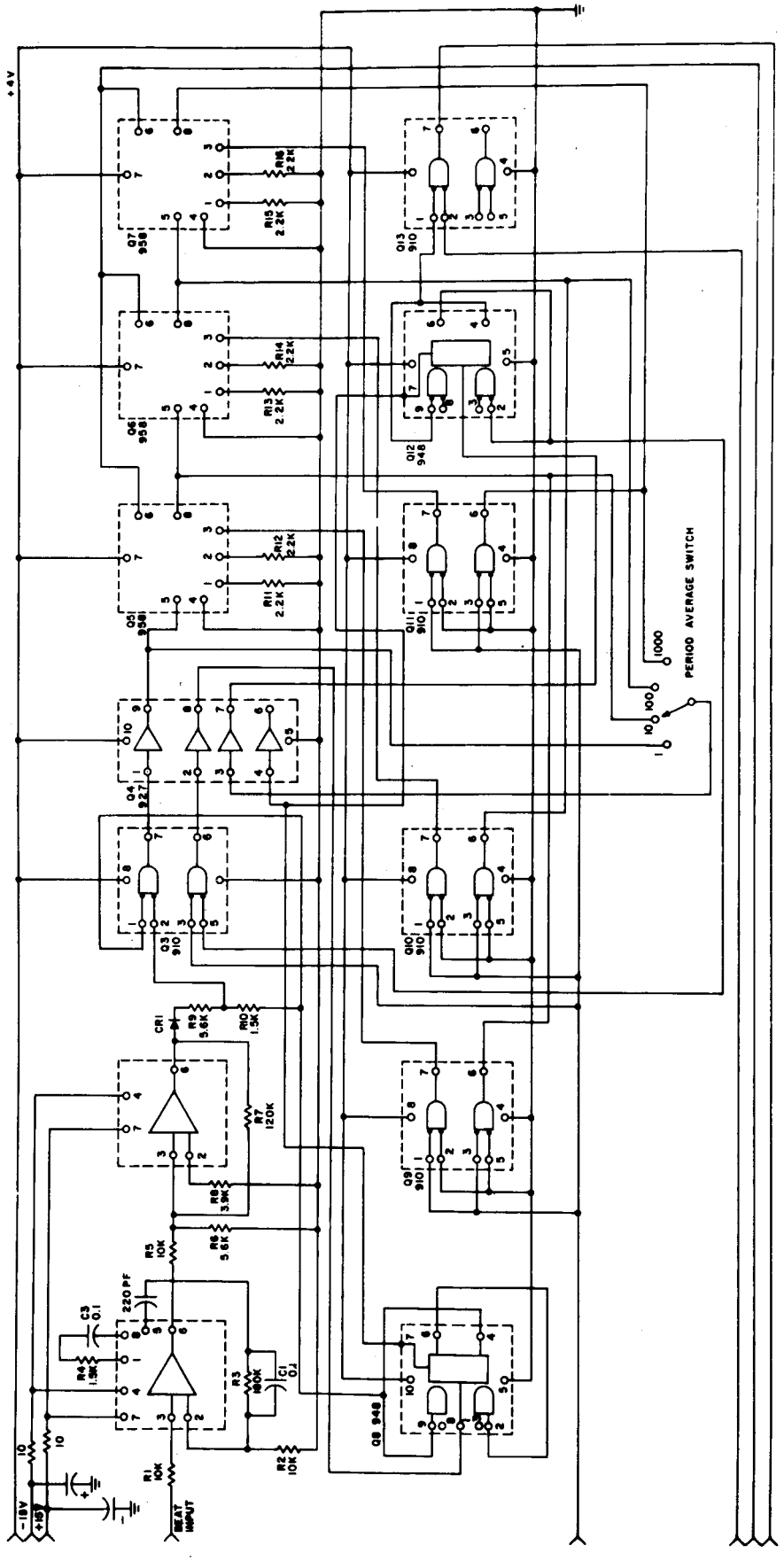

Fig. C-3. Period Gate Generator.

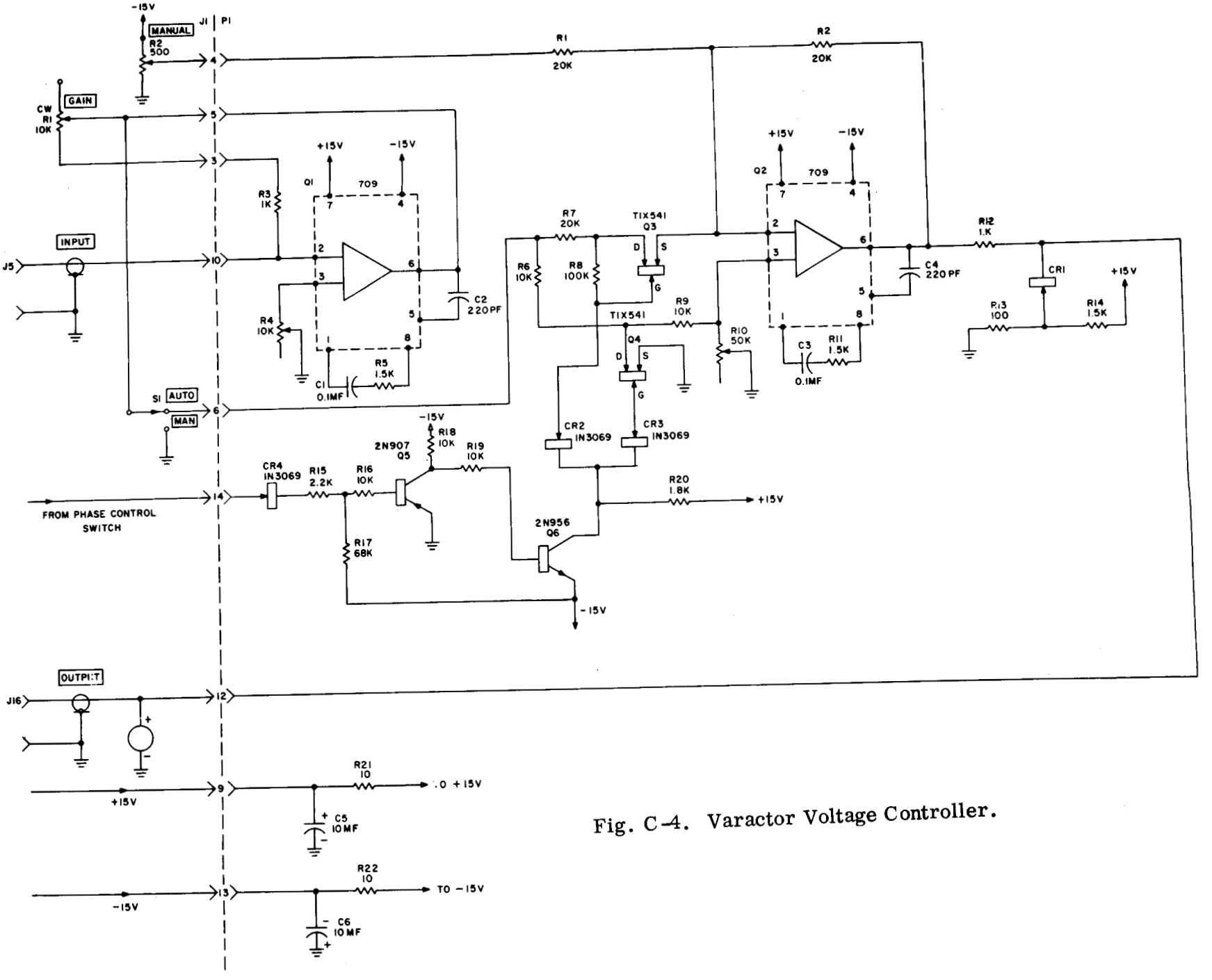

Fig. C-4. Varactor Voltage Controller.

Bidirectional Counter

The output of the period gate generator is a stream of pulses, at a 10 kHz rate, for an interval of 1, 10, 100 or 1000 periods of the beat between the two masers. The accumulated count on the bidirectional counter register is equal to the time duration of 1, 10, 100 or 1000 periods, respectively, measured in tenths of milliseconds.

The bidirectional counter itself is a standard commercial unit, Hewlett-Packard type 5280 A. The directional information to the counter is in the form of a d.c. logic level to channel B of the counter as shown in Fig. C-1; the command pulses from the master timer are converted to d.c. logic levels by integrated circuit bistable flip-flops in the count and polarity control unit; the circuitry is quite straightforward and need not be detailed here.

Digital-to-Analog Converter

The digital-to-analog converter is a standard General Radio type 1136A. Any three digits in the counter register can be transferred to the D-A register by the transfer command from the master timer. The digit transference is a "jam" transfer; the D-A register is not reset before the transfer command.

The analog voltage output from the D-A converter is always proportional to the count in the register. A transfer command is generated only once per timing cycle, after a full up and down count, so that the output of the D-A changes only once per cycle.

Varactor Voltage Controller

The output of the D-A converter goes to the summing terminal of the integrated circuit operational amplifier, Q1, in Fig. C-4. The gain of this stage, and therefore the loop gain of the servo, is adjustable by means of the variable feedback resistor R1.

The varactor diode is normally reverse-biased at the output of driver stage. Q2 must therefore always be positive with respect to ground. The "manual" control permits setting the quiescent output level of Q2 at any level between +1 and +14 volts. In order to obtain fully reversible feedback, it must be possible to increase or decrease the varactor voltage about the quiescent level set by the

"manual" control. The polarity control is accomplished by means of the FET analog gates Q3 and Q4. When Q3 and Q4 are closed, the feedback voltage is applied to the inverting terminal of Q3 and the correction voltage is added to the quiescent output of Q2. If Q3 and Q4 are open, the feedback voltage is applied to the noninverting terminal and subtracts from the quiescent voltage. The FET gates are ideally suited for this application as they have extremely low "on" resistances--in the order of 25 ohms, low leakage currents, and zero offset voltage. Furthermore, the series-shunt gate is designed to minimize input current offset of Q2.

The polarity information is carried by the sign of the count in the bi-directional counter register. The sign output from the counter is used to steer the analog gates at the input to Q2 so as to increase or decrease the varactor voltage. Since the counter register is also used for counting up and down, the sign output cannot be used directly to control the analog gates, but must be stored in a sign register, which is an integrated circuit J-K flip-flop physically located in the count and polarity control unit. After the bidirectional counter completes its up and down counting cycle, a polarity command from the master timer transfers the sign command from the sign register to the analog gates.

Pressure Control

The pressure control assembly is shown schematically in Fig. C-5. In the H-10 masers, the hydrogen pressure is set by applying a d.c. voltage to the Pirani gauge servo system. The pressure control assembly permits the presetting of two pressure levels by means of the ten-turn potentiometers labeled "Pressure 1" and "Pressure 2" and the remote selection of either pressure setting by means of the FET gates Q8 and Q9.

The integrated circuit bistable flip-flop, Q3, is triggered by the pressure control commands from the master timer. In state 1, Q3 turns off Q4 which turns off Q5. The gate of Q9 rises to the source voltage and Q9 is turned "on," connecting the wiper of the "Pressure 1" potentiometer to the maser. In the second channel Q6 and Q7 are turned on, which clamps the gate of Q8 at -15 volts and turns off gate Q8. In pressure state 2, the situation is reversed; Q8 is on and gate Q9 is off.

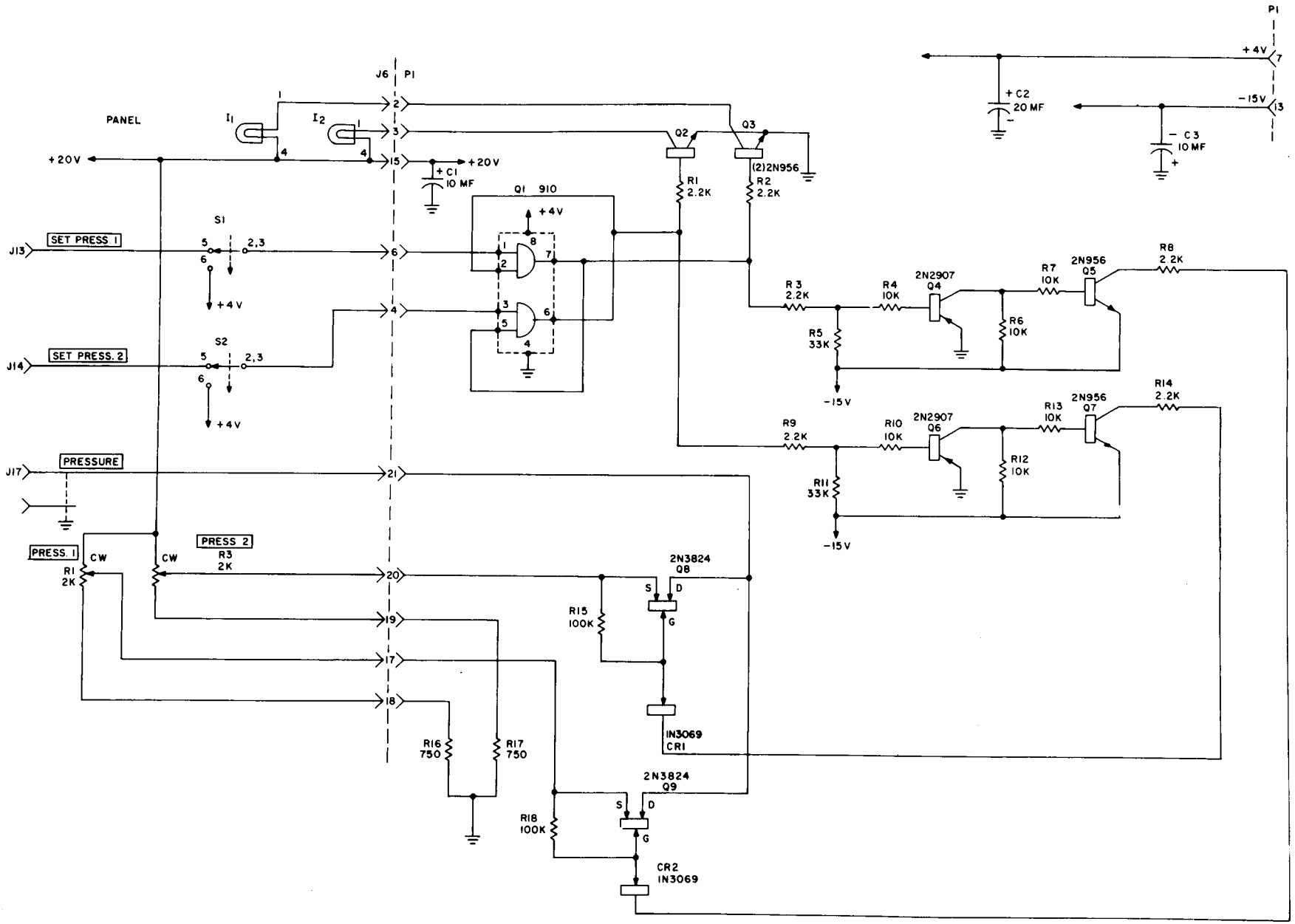

Fig. C-5. Pressure Control Assembly.

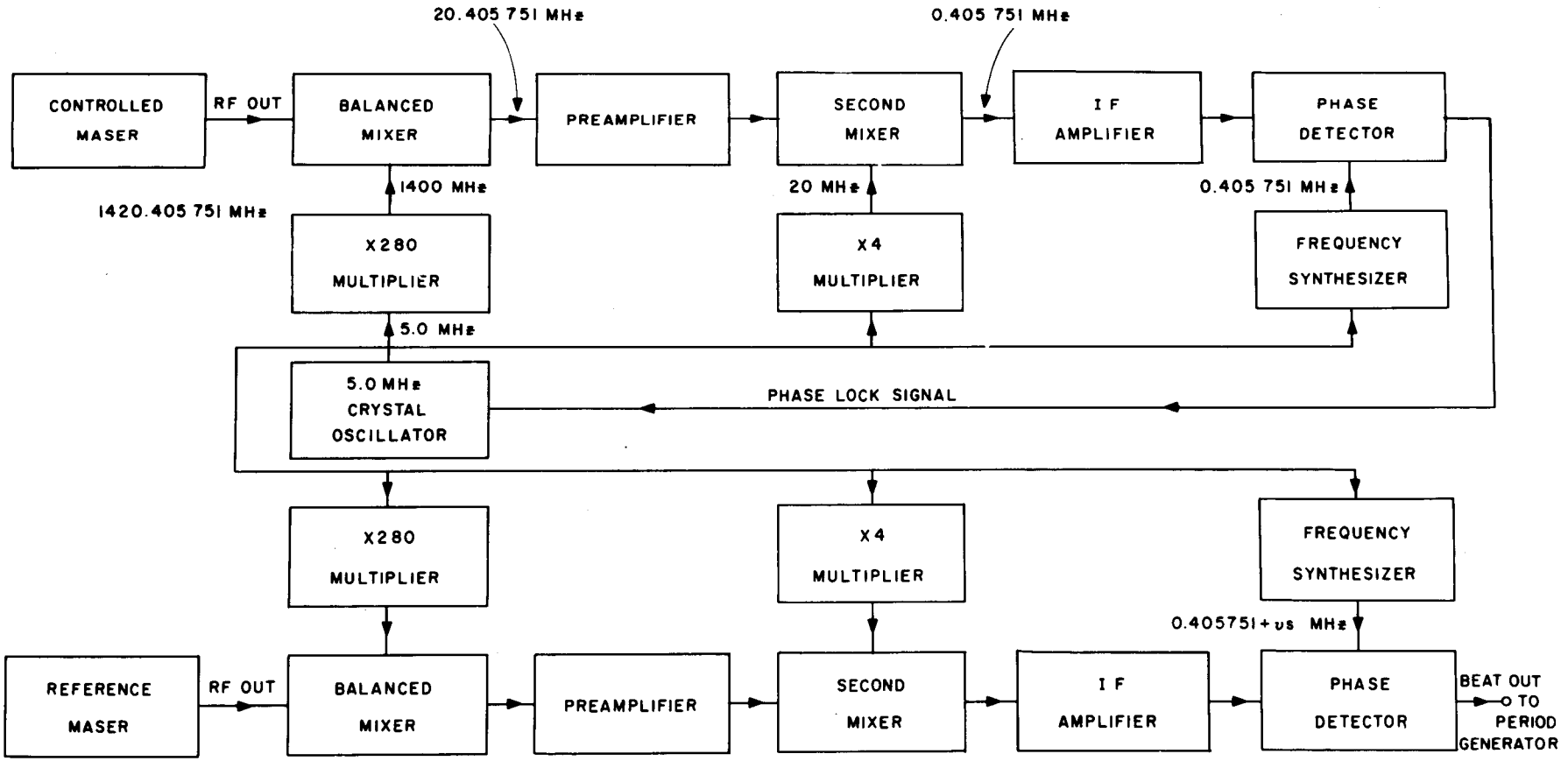

Fig. C-6. Block Diagram of Phase Lock Loop.

Phase Lock Loop

The phase lock loop, shown in block diagram form in Fig. C-6, provides for the generation of a standard, 5.0 MHz, signal locked to the controlled maser oscillation and provides for the offset beat between the controlled maser and the reference maser.

As can be seen from Fig. C-6, the output of the 5.0 MHz oscillator is multiplied to 1400 mc by a varactor multiplier chain and mixed in a balanced mixer with the controlled maser output at 1420.405751 MHz to generate the first IF, 20.405751 MHz. The 20.405751 MHz signal is amplified and beat down to 0.405751 MHz in a second mixer and amplified again. The 20.0 MHz mixing signal is derived from the 5.0 MHz oscillator by means of a separate x4 multiplier. The 0.405751 MHz IF is one input to the phase detector, the other input being the output of the synthesizer which, in turn, is locked to the 5.0 MHz oscillator. The output of the phase detector is fed back to a varactor tuner in the 5.0 crystal oscillator so as to lock the phase of the crystal oscillator to that of the maser.

The output of the reference maser is fed to the input of a second receiver, identical to that in the controlled maser loop. The 5.0 MHz drive for the multiplier chains and the locking frequency for the reference synthesizer are derived from the phase-locked crystal oscillator in the controlled maser loop. The output of the reference phase detector is fed to the input of the period gate generator.

The beat offset is obtained by offsetting the frequency settings of two synthesizers. It can be readily seen that if the two masers are oscillating at exactly the same frequency, a difference of ν_s in the frequencies of the two synthesizers results in a phase detector output at a frequency ν_s. If the two maser frequencies differ by an amount ν_D, where $\nu_D = \nu_{m_1} - \nu_{m_2}$, then the output of the phase detector will equal the algebraic sum of ν_s and ν_D;

$$\nu_{beat} = \nu_s + \nu_D = \nu_s - (\nu_{m_1} - \nu_{m_2}) \tag{5}$$

If ν_s is greater than ν_D, ν_{beat} does not change sign and no possible ambiguity can arise in the operation of the automatic tuner.

D. THE OPTIMAL BULB SHAPE

The oscillation conditions for the atomic hydrogen masers have been discussed in rather general terms by several papers in the literature.[2,7,8] An important parameter is the quantity q which has the following value:

$$q = \frac{\rho \bar{v}_r \hbar}{8\pi\mu_o^2} \frac{\gamma_t}{\gamma_b} \frac{I_{tot}}{I} \frac{1}{Q} \frac{V_c}{\eta V_b}$$

where

ρ is the spin exchange cross-section

$\bar{v}_r$ is the average relative velocity,

$\hbar$ is Planck's constant divided by 2π,

γ_t is relaxation rate of the atoms in the bulb,

$\frac{\gamma_t}{\gamma_b} = \frac{\gamma_b + \gamma_w}{\gamma_b + \epsilon\gamma_w}$ where γ_b is the geometrical escape rate of atoms from the bulb,

γ_w is the wall relaxation rate,

ϵ is the ratio of wall relaxation events due to recombination of atoms to the total wall relaxation; ϵ has been measured and is found to be equal to 1,

μ_o is the Bohr magneton,

I_{tot} is total flux of atoms entering the bulb,

I is the flux in the desired state for oscillation,

Q is the loaded quality factor of the cavity,

V_c is the cavity volume,

V_b is the bulb volume,

$$\eta \equiv \frac{\left[\frac{1}{V_b}\int H_z dv\right]^2}{\frac{1}{V_c}\int H^2 dv}$$

The quantity, q, defined as above can be expressed in terms of quantities involving the geometry of the bulb region where the atoms interact with the r.f. magnetic field. The quantity $S = \eta \frac{V_b}{V_c} Q = \eta' Q$ contains this information and can be described as a filling factor, η' times Q. In this

expression, Q is the total Q of the cavity resonator and is defined in the usual way as

$$Q = \frac{2\pi \text{ Stored Energy}}{\text{Energy lost per cycle by various means}}$$

and $\frac{1}{Q} = \frac{1}{Q_d} + \frac{1}{Q_w} + \frac{1}{Q_{ext}}$

Q_d includes only dielectric losses,
Q_w includes only wall losses,
Q_{ext} includes only power lost to outside circuitry.

The quantity q can be expressed in terms of a factor that involves fundamental constants and another factor involving geometry, and under the usual conditions for the hydrogen maser where the state selector focusses both the $F=1$, $m_F=0$ and $+1$ states, the value of q can be written

$$q = \frac{9.95 \times 10^2}{S}$$

For maser oscillation $q \leq 0.172$. For oscillation under the above conditions, $S \geq 5.78 \times 10^3$.

To obtain a value of S as large as possible the geometry of both the bulb and cavity must be considered with particular attention to the wall, dielectric and coupling losses.

In the present study the geometry of the cavity has been fixed to that of a right circular TE_{011} mode cavity. This cavity has a theoretical, unloaded Q of 87,000 and values of about 60,000 have been obtained in practice. The problem of determining the best shape of the bulb within this cavity and the value of η' due to this shape has been solved.

η' is defined as:

$$\frac{\left[\frac{1}{V_b}\int_b H_z\,dV\right]^2}{\left[\frac{1}{V_c}\int_c H^2\,dV\right]}\;\frac{V_b}{V_c} = \frac{\langle H_z\rangle_{bulb}}{\langle H^2\rangle_{cavity}}\;\frac{V_b}{V_c}$$

where H_z and H are the z component and total magnetic field of the oscillation in the maser cavity, b refers to the maser storage bulb, and c to the maser cavity.

Differentiation with respect to infinitesimal changes of bulb volume yields:

$$\frac{d\eta'}{dV_b} = \left\{\frac{2H_z)_{b\,surf}\left[\int_b H_z\,dV\right]}{V_b} - \frac{1}{V_b^2}\left[\int_b H_z\,dV\right]^2\right\}\frac{1}{\int_c H^2\,dV}$$

where $H_z)_{b\,surf}$ is the value of H_z at the point on the surface of the bulb where the infinitesimal volume change took place.

Thus

$$\frac{d\eta'}{dV_b} = \frac{\left[2H_z)_{b\,surf}\langle H_z\rangle_{bulb} - \langle H_z\rangle^2_{bulb}\right]}{V_c\,\langle H^2\rangle_{cavity}}$$

or

$$\frac{d\eta'}{\eta'} = \left(\frac{2H_z)_{b\,surf} - \langle H_z\rangle_{bulb}}{\langle H_z\rangle_{bulb}}\right)\frac{dV_b}{V_b}$$

This expression gives a criterion for determining how deformations of the bulb surface volume affect the filling factor. In particular, when $2H_z)_{b\,surf} = \langle H_z\rangle_{bulb}$, the filling factor is at its maximum value. This says that the optimal surface for the bulb is one for which H_z is a constant and that the maximum value of the filling factor occurs when the value of the average value of H_z within the bulb is twice its value on the surface. The value for H_z which satisfies this criterion has

been obtained by numerical methods in the case of a cylindrical cavity operating in the TE_{011} mode. It has been assumed that the bulb introduces no distortion of the field lines in the cavity, an obvious idealization.

In this case, we take the form of H_z to be normalized to:[9]

$$H_z(r,z) = \frac{k_1}{k} J_0(k_1 r) \cos(k_3 z) = \frac{k_1}{k} J_0(u) \cos(v),$$

where we change to variables $u = k_1 r$, $v = k_3 z$, $du = k_1 dr$, $dv = k_3 dv$. The volume element $4\pi r\,dr\,dz$ becomes $\frac{4\pi}{k_1^2 k_3} u\,du\,dv$. We wish to find that value of $H_z = \text{const.} = c_0 \frac{k_1}{k}$ such that $\langle H_z \rangle_{bulb} = 2c_0 \frac{k_1}{k}$. In performing the integrations, cos v goes between 0 and $c/J_0(u)$, u goes between 0 and $J_0(u) = c$.

Thus

$$\int_b H_z\,dV = \frac{4\pi}{k_1^2 k_3} \frac{k_1}{k} \iint J_0(u) \cos(v)\; u\,du\,dv$$

$$= \frac{4\pi}{k_1^2 k_3} \frac{k_1}{k} \int_0^{J_0(u)=c} J_0(u)\, u\,du \left[\sin v \right]_0^{\cos^{-1} \frac{c}{J_0(u)}}$$

$$= \frac{4\pi}{k_1^2 k_3} \frac{k_1}{k} \int_0^{J_0(u)=c} J_0(u)\, u\,du\, \frac{\sqrt{J_0^2(u) - c^2}}{J_0(u)}$$

$$= \frac{4\pi}{k_1^2 k_3} \frac{k_1}{k} \int_0^{J_0(u)=c} \sqrt{J_0^2(u) - c^2}\; u\,du$$

and

$$V_b = \int_b dV = \frac{4\pi}{k_1^2 k^3} \iint u\,du\,dv$$

$$= \frac{4\pi}{k_1^2 k_3} \int_0^{J_0(u)=c} u\,du \cos^{-1} \frac{c}{J_0(u)}$$

Hence

$$\langle H_z \rangle_{bulb} = \frac{\int_b H_z \, dV}{\int_b dV} = \frac{\frac{k_1}{k} \int_0^{J_0(u)=c} \sqrt{J_0^2(u) - c^2}\, u\, du}{\int_0^{J_0(u)=c} u\, du \cos^{-1} \frac{c}{J_0(u)}}$$

To optimize η', $\langle H_z \rangle_{bulb} = 2c_0 \frac{k_1}{k}$. Hence, we must find that value of c such that

$$2c_0 = \frac{\int_0^{J_0(u)=c} \sqrt{J_0^2(u) - c^2}\, u\, du}{\int_0^{J_0(u)=c} u\, du \cos^{-1} \frac{c}{J_0(u)}}$$

When c_0 satisfies this equation, then the corresponding value of η' is:

$$\eta'_{opt} = \frac{\langle H_z \rangle_b^2}{\langle H^2 \rangle} \frac{V_b}{V_c} = \frac{\left(2c_0 \frac{k_1}{k}\right)^2}{\langle H^2 \rangle} \frac{\frac{4\pi}{k_1^2 k_3} \int_0^{J_0(u)=c_0} u\, du \cos^{-1} \frac{c}{J_0(u)}}{\pi R^2 L}$$

$$= \frac{16}{\pi} \frac{1}{\langle H^2 \rangle} \frac{c_0^2}{x_{01}^2 + \frac{\pi^2 R^2}{L^2}} \int_0^{J_0(u)=c_0} u\, du \cos^{-1} \frac{c}{J_0(u)}$$

Approximating the surface $H_z = \text{const.}$ by an ellipsoid, we obtained an approximate value for $c_0 = .25$. We therefore evaluated the integrals

$$\int_0^{J_0(u)=c} \sqrt{J_0^2(u) - c^2}\, u\, du \qquad \text{and} \qquad \int_0^{J_0(u)=c} u\, du \cos^{-1} \frac{c}{J_0(u)}$$

numerically for values of $c = .26, .25, .24$. The integration method was Weddle's Rule and Simpson's Rule. Our results are as follows.

c	$\int_0^{J_0(u)=c} \cos^{-1}\frac{c}{J_0(u)}\, u\, du$	$\int_0^{J_0(u)=c} \frac{}{\sqrt{J_0^2(u)-c^2}}\, u\, du$	$2c\int_0^{J_0(u)=c} \cos^{-1}\frac{c}{J_0(u)}\, u\, du$	η'
.24	2.0156	1.00445	.96749	.4582
.25	1.9551	.99282	.97755	.4615
.26	1.8985	.97855	.98722	.4617
c_0 = .2565	1.9179	.9839	.9839	.4620 (R = L/2)

The value of c_0 was obtained from the first three rows by a second-order interpolation formula. ($x_{01} = 3.8317$, $\langle H^2 \rangle = .08111$.) The optimal value of η' was obtained for a cylindrical cavity whose diameter = its length (R = L/2). The value for η' for other values of R/L may be obtained by substitution in the term $x_{01} + \frac{\pi^2 R^2}{L^2}$ in the expression for η'_{opt}. The optimal bulb shape together with the best cylindrical and spherical bulb are shown in Figure D-1.

We also have determined the shape of the optimal outside bulb. The same criterion, to maximize η',

$$\langle H_z \rangle_{bulb} = 2\, H_z)_{b\ surf} = 2\, c_0$$

holds, and the integrals used in the preceding considerations appear in the same form. The limits of integration are altered, so that, e.g.,

$$\langle H_z \rangle_{bulb} = \frac{k_1}{k} \frac{\int_{u_0}^{x_{01}} \sqrt{J_0^2(u) - c^2}\, u\, du}{\int_{u_0}^{x_{01}} u\, du \cos^{-1}\frac{c}{J_0(u)}}$$

where the constant u_0 satisfies the equation $J_0(u_0) = c$. The estimated value of c_0 was about -.12. The result for an accurate numerical integration and interpolation is:

c	$\int_{u_0}^{x_{01}} \cos^{-1}\frac{c}{J_0(u)}\, u\, du$	$\int_{u_0}^{x_{01}} \sqrt{J_0^2(u) - c^2}\, u\, du$	$2c\int_{u_0}^{x_{01}} \cos^{-1}\frac{c}{J_0(u)}\, u\, du$	u_0	η'
-.12	4.3037	1.10335	1.0329	2.65	.2589
-.13	4.12952	1.08152	1.0737	2.672	.2593
c_0 = -.1313	4.10675	1.07855	1.07855		.2593

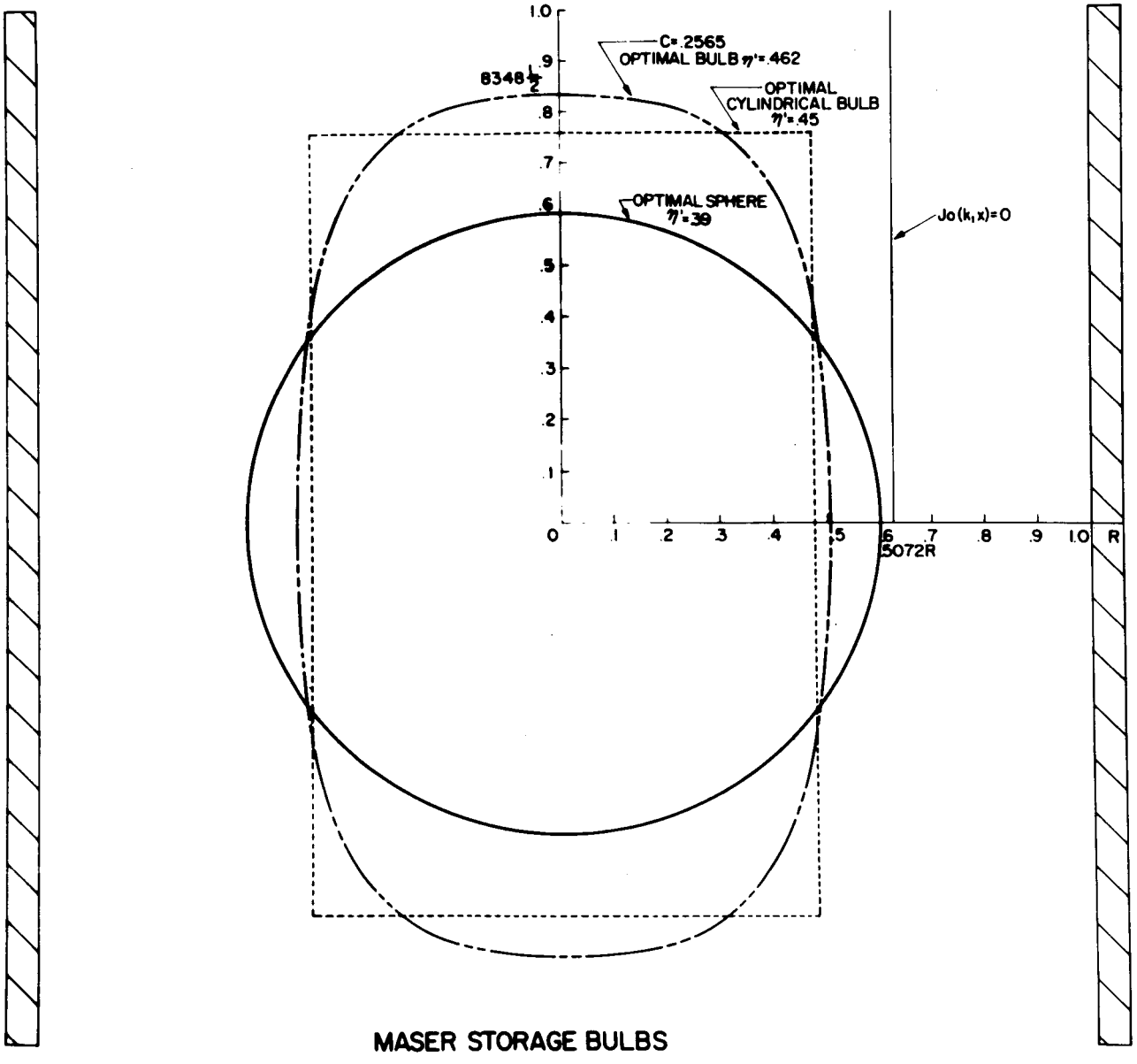

Fig. D-1. Optimal Bulb Shapes.

The optimal "football" and outside "doughnut" bulbs are shown in Figure D-2. If both these bulbs were pumped with hydrogen atoms, the total η' for both would be .7213. However, the wall collision rate in the outside bulb is higher than in the convex-shaped bulbs. The comparative figures are:

Optimal sphere: $\lambda = .8R$

Optimal cylinder: $\lambda = .726R$

Optimal outside bulb: $\lambda = .473R$.

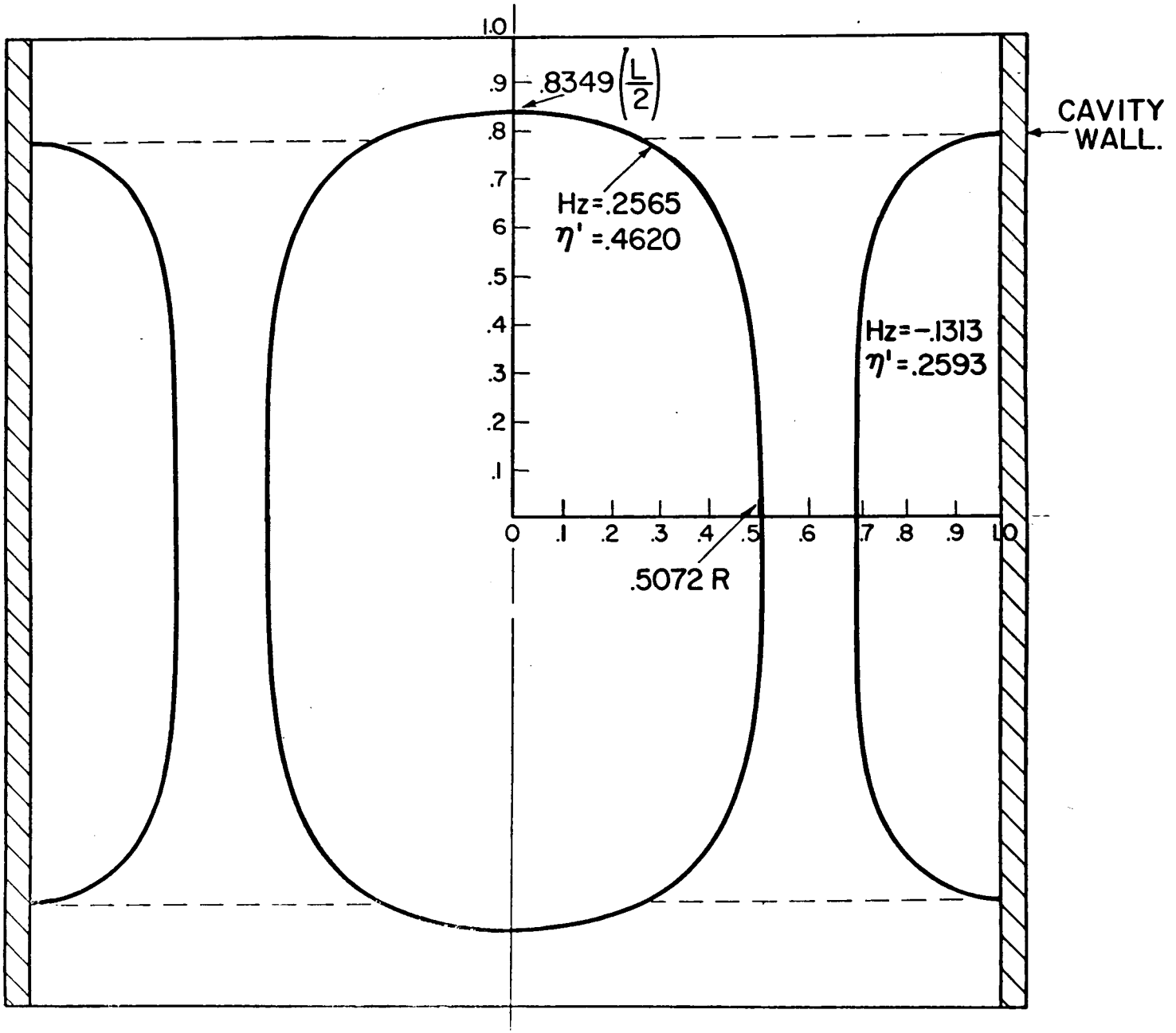

Fig. D-2. Optimal Convex and Outside Bulb Shapes.

III. THE RELATIONSHIP OF THESE STUDIES TO THE MASER PROGRAM AT THE GODDARD SPACE FLIGHT CENTER

The development of the hydrogen maser as a practical laboratory-based instrument has taken place in a relatively short period of time since the original discovery of the storage bulb principle. This occurred in 1960, and shortly afterward considerable effort was undertaken aimed at understanding the quantum mechanical effects. Later experiments consisted in making stability checks and improving the stability by the obvious means of controlling various parameters such as magnetic field temperature, cavity tuning, etc. The results obtained from these early time-keeping experiments were very encouraging and, when further studies on maser theory and techniques were done, considerable improvement was made essentially in the areas where the physics of the instrument was involved.

Relatively little change in the configuration of the maser had occurred until the time when the present study was begun. An r.f. discharge dissociator, a relatively standard hexapole and a relatively standard bulb constituted the "standard" maser. The need for a more reliable dissociator became obvious due to the instabilities and inconveniences of the r.f. discharge. The lengthy and tedious tuning procedure requiring a skilled operator was also a deterrent to the use of the maser as a piece of field equipment. Renewed interest in the gravitational red shift experiment involving a satellite maser made further requirements on the design of the maser; questions of size, weight and power were being raised.

The present study contract was directed to investigating and evaluating techniques leading to improved hydrogen masers with attention to the elimination of the r.f. interference from the discharge dissociator and to the goal of simplifying the lengthy cavity tuning process. Improvements were designed to be tested on two government-furnished masers, and the criteria of the design of the hardware improvements were to emphasize the application of the maser to field and space use. This work was to be done keeping in mind possible retrofitting of the NASA/GSFC masers using similar design improvements.

The work in the improvement of the dissociator was originally motivated by r.f. inteference problems; however, as the study has progressed, it appears that the

thermal dissociator is capable of more complete dissociation, probably close to 95%. The r.f. dissociator is likely to be less than half as efficient, chiefly due to recombination in the beam collimator. Since the collimator of the thermal dissociator is hot, this effect is not a problem. The evolution of the dissociator from the directly heated version requiring very high power to the electron bombardment heated version requiring far less power has been discussed, and the description of a design arising from work continued in a further contract, NASW-1337, is given. This information and further information as it comes to light in the course of the above program may be of use in retrofitting the NASA/GSFC masers.

A study of the beam trajectories in the focussing magnet was undertaken for two reasons. First, the greater thermal velocities from the thermal dissociator made necessary a recalculation of the magnet configuration. This could have been done, as previously for the r.f. dissociator, in a relatively rough manner. However, other factors became important, such as the possibility of eliminating bulb pollution and other undeflected particles in the beam by using a stopping disc at the exit aperture of the magnet. For a short apparatus, this can be a serious problem. A computer program was developed to calculate trajectories and give beam intensities for various geometrical conditions. The results have shown that, while the rough approximation previously used is not bad, it is possible to design an optimum configuration where it should be possible to predict the flux entering the bulb within a few per cent. The optimizing of maser performance with respect to beam flux is important for several reasons:

1) Pump lifetime is proportional to total hydrogen flux into the maser. Hydrogen should be dissociated as efficiently as possible, state selected and focussed as effectively as possible into the bulb.

2) By proper design of the r.f. interaction region, the oscillation of the maser can be achieved with a minimum flux into the bulb.

3) The condition for having the lowest flux threshold also allows the best tuneability.

This last condition can be described best in terms of the parameter q discussed in the section on the optimum bulb shape. The ratio, r, of the maximum

linewidth to the minimal linewidth of the atomic resonance is given in terms of q

$$r = \frac{1 + q + 1\,(1 - 6q + q^2)^{1/2}}{1 + q - (1 - 6q + q^2)^{1/2}}$$

The smaller the value of q the better, so that by raising the pressure of the atoms in the storage bulb the linewidth of the atomic transition is broadened due to spin exchange collisions among the atoms. The process must not, however, prevent the maser from oscillating. Cavity-bulb geometries providing a small value of q hence are favorable in many ways to the successful operation of the atomic hydrogen maser.

An important part of the program has been the study of automatic tuning techniques. Prior to the beginning of the program, several techniques had been considered to set the cavity to the correct maser frequency. It was decided that techniques using external power to probe the resonant cavity and set it to resonance had disadvantages. One of these is the required phase and amplitude stability of the microwave bridge measuring the impedance of the cavity as observed from the reflected amplitude and phase of the probing signal. Further, the probing signals can severely perturb the maser oscillation unless the signals are of very small level and are applied symmetrically about the center value of frequency where the maser is expected to oscillate. The line broadening method had been selected because it does not depend on any à priori knowledge of the cavity frequency and leads automatically to a condition where the maser is tuned in such a way as to remove certain types of systematic shifts of frequency that are proportional to the linewidth.[10] The most important of these is the effect of frequency shifts due to atom collisions in the bulb as calculated by Bender.[11]

The use of linewidth modulation by spin exchange offers a particular advantage in that the ratio of the maximum to minimum linewidths can be made greater than by using other techniques for line broadening such as magnetic gradient quenching or a foreign gas as a quenching medium.

Having thus decided on the technique, reference oscillators other than hydrogen masers were considered for observing the necessarily small frequency

shifts that result from this technique. Some information about crystal oscillators had been obtained as a result of previous involvement in measurements and techniques for measuring short term stability. The use of a very stable crystal oscillator and long integration "lock-in" techniques for seeking out a small shift coherent with an applied quenching had been considered. In spite of the obvious cost advantages in having but one maser in such a system, the requirements of long integration times and the uncertainties in the performance of crystal oscillators made this method a doubtful one, expecially if one considered the probable aims of any programs involving hydrogen masers. These aims are to provide the ultimate in frequency reproducibility and stability for measurements that cannot be made by any other standard. The use of two independently operating masers in such a measuring system seems obvious, since it is usually necessary to obtain assurance of the stability of the system. The tuning method using the line broadening technique employing two masers operates each as an independent unit. The reference maser can be operated with a randomly chosen frequency offset; the only requirement is that it should operate with frequency stability comparable to that of the maser being tuned. The successful automation of this method thus provides not only a stable oscillator continuously verified to be operating close to its ideal frequency, but also a measure of the performance of the oscillator. The performance can be evaluated by monitoring the difference frequency between the masers and employing the appropriate statistical methods.

IV. NEW TECHNOLOGY

The following are areas where advances have been made in technology:

a) Thermal dissociator for atomic hydrogen maser;
   i. Direct heating by electric current
   ii. Electron bombardment heating

b) The establishment of optimum configurations of bulb structures for cylincrical TE_{011} mode resonators;
   i. Optimal shape of bulb
   ii. Optimal sphere

c) An automatic tuning technique for stabilizing the output frequency of the maser to the resonance frequency of the hydrogen atom confined in the maser bulb.

Patent disclosures have been written for these new techniques.

REFERENCES

1. For a survey of the variety of sources, see Bass & Broida, Formation and Trapping of Free Radicals, Academic Press, p. 47 (1960).

2. Kleppner, Berg, Crampton, Ramsey, Vessot, Peters and Vanier, Phys. Rev. 138, A972 (1965).

3. Tables of Thermal Properties of Gases, NBS Circular 564 (1955).

4. W. Lamb and R. C. Retherford, Phys. Rev. 79, 549 (1950); 81, 222 (1951).

5. M. Eisenstadt, Rev. Sci. Instr. 36, 1878 (1965).

6. J. Vanier and R. F. C. Vessot, Appl. Phys. Letters, 4:7, 122 (1964).

7. D. Kleppner, H. M. Goldenberg and N. F. Ramsey, Phys. Rev. 126, 603 (1962).

8. H. M. Goldenberg, D. Kleppner and N. F. Ramsey, Phys. Rev. 123, 530 (1961).

9. Montgomery, Technique of Microwave Measurements, M. I. T. Rad. Lab. Series, No. 11, p. 299.

10. S. B. Crampton, D. Kleppner and N. F. Ramsey, Phys. Rev. Letters 11, 338 (1963).

11. P. L. Bender, Phys. Rev. 132, 2154 (1953).

DISTRIBUTION LIST

Goddard SFC/NASA
Greenbelt, Md. 20771

1- Office of Director, Code 100

3- Office of Asst. Dir. SS&A, Code 600

3- Office of Asst. Dir. T&DS, Code 500

3- Office of Technical Services, Code 300

2- Library, Code 252

1- Contracting Officer, Code 248
Attn: Wm. P. Danbury

4- Technical Information Div., Code 250

3- Technical Director, Code 521
Attn: A.R. Chi

Marshall SFC/NASA
Huntsville, Alabama
Attn: John J. Gregory
R-ASTR-IRT

Jet Propulsion Laboratory
Calif. Institute of Technology
4800 Oak Grove Drive
Pasadena, California
1- Attn: Dr. R. Sydnor
1- Attn: Mr. W. Higa

National Bureau of Standards
U.S. Dept. of Commerce
Boulder, Colorado
Attn: F. R. Petersen

Joint Institute for Laboratory
Astrophysics (JILA)
University of Colorado
Boulder, Colorado
Attn: Dr. P. Bender

Wright-Patterson AFB
Dayton, Ohio
Attn: Mr. Charles Friend,
AFAL (AVNT)

U.S. Army Electronics Command
Solid State & Frequency Control Div.
Fort Monmouth, New Jersey 07703
Attn: R. V. McKnight,
AMSEL-KL-SM

Bureau of Ships
Dept. of the Navy
Washington, D.C.
Attn: Mr. M. H. Criswell,
Code 681A2

Navy Electronics Laboratory
San Diego 52, California
Attn: Mr. C. J. Casselman
VLF Techniques Div., Code 3240

Naval Research Laboratory
Washington, D.C.
Attn: Dr. R. R. Stone

Office of Naval Research
Washington, D.C.
Attn: Dr. A. Shostak
Electronics Br., Code 427

Prof. N. F. Ramsey
Lyman Laboratory of Physics
Harvard University
Cambridge, Mass.

Prof. C. H. Townes
Physics Dept.
Mass. Institute of Technology
Cambridge, Mass. 01239